A positively tuned voltage indicator for extended electrical recordings in the brain

S. Wenceslao Evans[1,23], **Dong-Qing Shi**[2,23], **Mariya Chavarha**[3,23], **Mark H. Plitt**[1], **Jiannis Taxidis**[4,5,6], **Blake Madruga**[4], **Jiang Lan Fan**[7], **Fuu-Jiun Hwang**[8], **Siri C. van Keulen**[10,11,12], **Carl-Mikael Suomivuori**[10,11,12], **Michelle M. Pang**[1], **Sharon Su**[1], **Sungmoo Lee**[1], **Yukun A. Hao**[1,3], **Guofeng Zhang**[1], **Dongyun Jiang**[1], **Lagnajeet Pradhan**[1], **Richard H. Roth**[8], **Yu Liu**[8,9], **Austin Reese**[13], **Adrian Negrean**[13], **Attila Losonczy**[13,14], **Christopher D. Makinson**[13,15], **Sui Wang**[9], **Thomas R. Clandinin**[1], **Ron O. Dror**[10,11,12], **Jun B. Ding**[8,16], **Na Ji**[5,17,18,19,20], **Peyman Golshani**[4,21], **Lisa M. Giocomo**[1], **Guo-Qiang Bi**[2,22], **Michael Z. Lin**[1,3,*]

[1]Department of Neurobiology, Stanford University Medical Center, Stanford, CA, USA

[2]Division of Life Sciences and Medicine, University of Science and Technology of China, Hefei, China

[3]Department of Bioengineering, Stanford University, Stanford, CA, USA

[4]Department of Neurology, UCLA David Geffen School of Medicine, Los Angeles, CA, USA

[5]Program in Neurosciences & Mental Health, Hospital for Sick Children, Toronto, Ontario, Canada

[6]Department of Physiology, University of Toronto, Toronto, Ontario, Canada

[7]UC Berkeley/UCSF Joint Program in Bioengineering, University of California Berkeley, Berkeley, CA

[8]Department of Neurosurgery, Stanford University Medical Center, Stanford, CA, USA

[9]Department of Ophthalmology, Stanford University Medical Center, Stanford, CA, USA

[10]Department of Computer Science, Stanford University, Stanford, CA, USA

[11]Departments of Structural Biology and of Molecular and Cellular Physiology, Stanford University School of Medicine, Stanford, CA, USA

[12]Institute for Computational and Mathematical Engineering, Stanford University, Stanford, CA, USA

[13]Department of Neuroscience, Columbia University, New York, NY, USA, Mortimer B. Zuckerman Mind Brain Behavior Institute, New York, NY, USA

[14]Kavli Institute for Brain Science, New York, NY, USA

[15]Institute for Genomic Medicine, Columbia University, New York, NY, USA, Department of Neurology, Columbia University, New York, NY, USA

[16]Department of Neurology and Neurological Sciences, Stanford University Medical Center, Stanford, CA, USA

[17]Department of Molecular and Cell Biology, University of California Berkeley, Berkeley, CA

[18]Department of Physics, University of California Berkeley, Berkeley, CA

[19]Helen Wills Neuroscience Institute, University of California Berkeley, Berkeley, CA

[20]Molecular Biophysics and Integrated Bioimaging Division, Lawrence Berkeley National Laboratory, Berkeley, CA, USA

[21]Semel Institute for Neuroscience and Human Behavior, David Geffen School of Medicine, UCLA, Los Angeles, CA, USA

[22]Interdisciplinary Center for Brain Information, Brain Cognition and Brain Disease Institute, Shenzhen Institute of Advanced Technology, Chinese Academy of Sciences, Shenzhen, Guangzhou, China.

[23]These authors contributed equally

Abstract

Genetically encoded voltage indicators (GEVIs) enable optical recording of electrical signals in the brain, providing subthreshold sensitivity and temporal resolution not possible with calcium indicators. However, one- and two-photon voltage imaging over prolonged periods with the same GEVI has not yet been demonstrated. Here, we report engineering of ASAP-family GEVIs to enhance photostability by inversion of the fluorescence-voltage relationship. Two of the resulting GEVIs, ASAP4b and ASAP4e, respond to 100-mV depolarizations with 180% fluorescence increases, compared to the 50% fluorescence decrease of the parental ASAP3. With standard microscopy equipment, ASAP4e enables single-trial detection of spikes *in vivo* over the course of minutes. Unlike GEVIs previously used for one-photon voltage recordings, ASAP4b and ASAP4e also performs well under two-photon illumination. By imaging voltage and calcium simultaneously, we show that ASAP4b and ASAP4e can identify place cells and detect voltage spikes with better signal-to-noise ratios and temporal resolution than commonly used calcium indicators. Thus, ASAP4b and ASAP4e extend the capabilities of voltage imaging to standard one- and two-photon microscopes while improving the duration of voltage recordings.

Recording the real-time activity of genetically specified neurons during behavior will be crucial for understanding how the nervous system relays and processes information[1,2]. Currently, most genetically specified activity recording is performed using fluorescent genetically encoded calcium indicators (GECIs). Detection of calcium activity is aided by high expression levels of GECIs, low fluorescence at baseline, and the high amplitude and long duration of calcium transients following action potentials (APs). However, GECI signals lack precise timing of spikes, as calcium continues rising after the AP peak due to delayed inactivation of voltage-gated calcium channels and continued diffusion from initial influx points into the cytosol[3,4]. This spatiotemporal smoothing effect, together with >200-ms half-extrusion times for calcium, prevents GECIs from accurately discerning closely spaced APs[2]. Lastly, calcium levels do not respond appreciably to subthreshold and hyperpolarizing changes in transmembrane voltage, and thus do not reveal subthreshold dynamics such as theta rhythms and hyperpolarizing events.

Genetically encoded voltage indicators (GEVIs) can more accurately time spikes and reveal subthreshold dynamics than GECIs. However, voltage imaging suffers from intrinsic signal detection challenges not suffered by calcium imaging. GEVIs must exist at the membrane to report voltage changes, resulting in fewer molecules per imaging volume compared to cytosolic GECIs[5]. In addition, as electrical events are much faster than calcium events, GEVIs that track electrical kinetics produce shorter-lived signals than GECIs. This limits the number of integrated photons per transient while necessitating faster sampling rates for response detection compared to calcium imaging. For example, the GEVI ASAP3 produces a similar relative fluorescence change (F/F_0) to a single AP as the widely used GECI GCaMP6f (~20%), and actually does so with ~20-fold higher per-molecule brightness[6]. However, its abundance per cell body is estimated to be ~20-fold lower, while its responses are 20-fold shorter in duration[6].

To combat these formidable challenges, GEVI engineering over the last several decades has focused on increasing the per-molecule change in fluorescence upon voltage change and optimizing kinetics. In particular, brighter fluorophores and faster onset kinetics improve responses in absolute photons per molecule, while slightly slower offset kinetics improve detectability by extending the response. Currently, the GEVIs with the largest relative response per AP are Archon1 and ASAP3. Archon1 consists of a non-conducting opsin domain and demonstrates voltage-dependent fluorescence upon red light illumination, due to absorbance shifting by voltage-dependent retinal Schiff base protonation. As the inherent fluorescence of opsins is dim, intense illumination is required to detect them[7]. Opsins can be fused to a brighter fluorophore, allowing the fluorophore brightness to be modulated by FRET in a voltage-dependent manner, but the degree of modulation is limited[8–11]. Both types of opsin-based GEVIs show poor responsivity under two-photon illumination, likely because voltage sensitivity resides in a transient state of the opsin photocycle that is inefficiently interrogated with two-photon excitation[5,12,13].

In contrast to opsin-based GEVIs, ASAP3 responds equally well under one- and two-photon illumination[6,12]. ASAP3 is composed of a circularly permuted GFP (cpGFP) inserted in an extracellular loop of a voltage-sensing domain (VSD), so that voltage-dependent VSD movements are transduced to modulate cpGFP fluorescence[6,14], analogously to cpGFP-

based indicators such as GCaMP (Fig. 1a). ASAP3 features a 51% fluorescence decrease with depolarization from −70mV to +30mV and sub-millisecond activation kinetics at 37 °C, as well as fortuitously inactivation kinetics of several millisconds[6]. Together, these characteristics result in the highest power-normalized signal-to-noise ratio for spikes and subthreshold events among GEVIs[15]. However, reported *in vivo* uses of ASAP-family GEVIs has only involved two-photon microscopy to date. In addition, rapid loss of ASAP3 fluorescence (50% in ~6 s) during two-photon raster scanning suggests that photostability may be a limiting factor in frame-illumination methods[16].

We set out to enhance the performance of ASAP-family GEVIs when using commonly available one- and two-photon imaging methods. In particular, we sought to improve photostability of ASAP-family GEVIs to enable long-duration whole-frame one- and two-photon recordings. Here, by combining computational protein modeling with our recently developed methods of PCR transfection and electroporation-induced membrane depolarization[6,17], we develop a positively tuned GEVI, ASAP4e, with a response amplitude of 210% in the physiological range and 468% over all voltages. ASAP4e also features enhanced photostability compared to ASAP3 under one- and two-photon illumination. We demonstrate that ASAP4e reports APs and sub-threshold oscillations in mice using standard one- or two-photon equipment. By simultaneously imaging with a red GECI, we also verify that ASAP4e provides higher temporal resolution with better SNR for single APs.

RESULTS

Engineering of positively tuned GEVIs.

A rational strategy to photostability improvement is to invert the voltage response of ASAP-family GEVIs to produce positive fluorescence changes with depolarization. This way, the GFP chromophore can reside in a low-fluorescence state at the negative transmembrane voltages of a resting neuron, either due to low absorption of excitation light or preponderance of non-radiative decay pathways from the excited state, which should be associated with slower photobleaching compared to higher-fluorescent chromophore states.

As with most other GFP-based indicators, ASAP-family GEVIs are imaged by excitation with ~490-nm light in one-photon mode or ~950-nm light with two-photon illumination. This wavelength selectively excites the deprotonated anionic form of the GFP chromophore with peak absorbance at ~490 nm, avoiding the protonated or neutral GFP chromophore with peak ~390-nm absorbance[18,19]. In wild-type GFP, hydrogen bond donation by His-148 (His-151 in ASAP variants) stabilizes the deprotonated state. We hypothesized that depolarization-induced movements in the S4 transmembrane helix cause ASAP dimming by disrupting hydrogen bond donation by His-151. Correspondingly, to invert the relationship between S4 movement and chromophore protonation, we targeted His-151 and neighboring amino acids (Fig. 1a).

Starting with ASAP2f L146G S147T R414Q, an intermediate in ASAP3 evolution[6], we first constructed and tested all 400 possible amino acid combinations at positions 150 and 151 by 384-well PCR transfection followed by automated electroporation and imaging [6]. We identified several mutants with upward responsivity (Extended Data Fig. 1), one of which,

S150D H151G (ASAP4.0), demonstrated a ~100% increase in fluorescence upon voltage steps from −70 mV to +30 mV, thereby inverting the response relative to ASAP3 (Extended Data Fig. 2a). However, ASAP4.0's fluorescence-vs-voltage (*F-V*) curve was right-shifted, such that the physiological voltage range of −70 to +30 mV mapped to the shallow lower portion of the curve (Extended Data Fig. 2b). As a result, the fluorescence change from −70 to +30 mV (F_{100}) was only 29% of the maximum obtainable fluorescence across all voltages (F_{max}), and the fluorescence at +30 mV (F_{+30}) was less than half of F_{max} (Extended Data Fig. 2b). In addition, ASAP4.0 responses demonstrated partial reversion during depolarization steps (Extended Data Fig. 2a), suggesting a relaxation process that reduces the proportion of activated molecules and/or shifts a proportion to a dimmer conformation.

Over four rounds of structure-guided mutagenesis of ASAP4.0, we were able to left-shift and sharpen the *F-V* curve, producing large responses in the physiological voltage range. Briefly, to reduce the rapid relaxation and obtain higher F_{+30}/F_{max}, we mutated a chromophore-interacting site in ASAP4.0 to increase chromophore rigidity[20]. One mutant, ASAP4.1, showed less relaxation (Extended Data Fig. 2a) but higher fractional fluorescence at rest ($F_{−70}/F_{max}$), resulting in reduced $F_{100}/F_{−70}$ (Extended Data Fig. 2b). We then performed double-site saturation mutagenesis at positions 148 and 149 in the linker between the third transmembrane helix of the VSD (S3) and cpGFP (Extended Data Fig. 2c), obtaining ASAP4.2 with an improved $F_{100}/F_{−70}$ and lower $F_{−70}/F_{max}$ (Extended Data Fig. 2b). Finally, by developing an atomic model of ASAP4.2, we identified Phe-413 at the end of the fourth transmembrane helix (S4) as a site that could modulate the energetic barrier to voltage-induced movements[21]. Mutation of Phe-413 revealed F413A, F413G, and F143M to have the largest relative responses to depolarization (Extended Data Fig. 3a). By testing responses over their full voltage-sensitivity range (Fig. 1b), we determined F413G and F413M had steeper *F-V* curves than F413A (Extended Data Fig. 3b), with $F_{100}/F_{−70}$ values of 180% and 210% respectively (Fig. 1b, Supplementary Table 1). Further details and rationale of protein engineering are in the Supplementary Note.

Among fully genetically encoded voltage indicators with high fluorescence, only ElectricPk, FlicR1, Marina and upward Ace2N-mNeon are positively tuned[9,15,22]. Like ASAPs, ElectricPk, FlicR1, and Marina are based on fusions of a VSD with a fluorescent protein domain, while upward Ace2N-mNeon is based on electrochromic FRET between the mNeonGreen fluorescent protein and a voltage-sensing opsin. Among these, Marina has the largest reported $F_{100}/F_{−70}$ at 29%. The positive indicator Ace2N-mNeon recently demonstrated single-AP detection, but no *F-V* curve was reported[9]. To allow comparison, we measured its *F-V* curve as well, obtaining $F_{100}/F_{−70}$ of 12% (Fig. 1b). Thus, ASAP4.2 F413G and ASAP4.2 F413M report physiological voltage changes with larger responses than previously described positively tuned GEVIs[23]. Given their optical characteristics, we named ASAP4.2 F413G as ASAP4b (brighter baseline) and ASAP4.2 F413M as ASAP4e (enhanced response).

Characterization of ASAP4 brightness and photostability.

As ASAP4.2 and later variants share an identical GFP chromophore environment, their maximum obtainable fluorescence per molecule should be similar. Fluorescence at a given voltage relative to maximal fluorescence across all voltages should then scale with per-molecule brightness at that voltage. Between ASAP4b and ASAP4e, ASAP4b exhibited higher molar brightness at both −70 mV and +30 mV, while ASAP4e exhibited a larger relative change due to lower brightness at −70 mV (Extended Data Fig. 3c). Both reached >50% of maximum fluorescence at +30 mV. While previous studies measured F-V curves at room temperature only, we also measured them for ASAP3, ASAP4b, and ASAP4e at 37 °C. Interestingly, ASAP4b and ASAP4e responses steepened and converged, due to lower F_{-70}/F_{max} for ASAP4b and higher F_{+30}/F_{max} for ASAP4e, while the F-V curve for ASAP3 underwent a left-shift (Extended Data Fig. 3c).

Per-cell brightness of an indicator will be influenced not just by voltage tuning, but also by total chromophore levels per cell which in turn depend on protein expression and chromophore maturation efficiency. To rule out issues with expression or maturation of ASAP4b or ASAP4e, we compared brightness of cells expressing ASAP3, ASAP4b, or ASAP4e with cells expressing ncpASAP4b, a protein composed of the VSD of ASAP4b with a non-circularly permuted version of the ASAP4b/4e GFP moiety in the S3-S4 loop. The GFP moiety in ncpASAP4b should be voltage-independent, as observed for other non-pHluorin non-permuted GFP fusions with VSDs[9,15,22,22,24], and thus serve as a proxy for the fluorophore of ASAP4b/4e in the maximally bright state. We found that cells expressing ASAP3, ASAP4b, and ASAP4e had 47%, 21%, and 17%, respectively, of the brightness of cells expressing ncpASAP4b (Extended Data Fig. 3d). These numbers agree well with the F_{-70}/F_{max} values of ASAP3, ASAP4b, and ASAP4e (Extended Data Fig. 3c), indicating that total chromophore levels per cell are similar between these three GEVIs.

In GCaMP GECIs, calcium induces brightening upon one-photon excitation at ~490 nm by shifting the chromophore population from a protonated ~390 nm-excitable state to a deprotonated ~490 nm-excitable state[25]. At resting membrane potentials near −70 mV, ASAP4.2 F413G and F413M exhibit less than 30% of their maximal fluorescence at room temperature, compared to about 50% for ASAP3 (Extended Data Fig. 3c). If these differences are also due to protonation, then we would expect ASAP4.2 F413G and F413M to have a higher 380/490-nm excitation ratio compared to ASAP3 at rest. Indeed, excitation spectra a shift to the 390 nm-excitable state for ASAP4.2 F413G and F413M compared to ASAP3 (Extended Data Fig. 3e), consistent with the prediction. In addition, ASAP4.2 F413G and F413M show a red-shift in emission, which is explained by the introduction in ASAP4.1 of T206H, a mutation known to red-shift the Clover subfamily of GFPs[20]. Under two-photon illumination, ASAP3, ASAP4b, and ASAP4e are all maximally excited at 938 nm (Extended Data Fig. 3f).

We next compared photostability under one-photon or two-photon illumination for ASAP4b, ASAP4e, and ASAP3. Under 453-nm one-photon illumination at 9 to 450 mW/mm^2, ASAP3 and ncpASAP4b photobleached monotonically (Extended Data Fig. 4a). In contrast, ASAP4b and ASAP4e exhibited photoactivation at all powers, and photobleached at later times at higher powers (Extended Data Fig. 4a). ASAP4b and ASAP4e were also more

photostable under higher-intensity two-photon illumination than ASAP3 (Extended Data Fig. 4b). Most of the two-photon photobleaching represented reversibly photoswitchable events, as a few minutes of incubation in the dark led to recovery of the majority of the lost fluorescence (Extended Data Fig. 4c).

Reporting of fast voltage dynamics by ASAP4.

To understand how well ASAP4b and ASAP4e can report voltage dynamics of different speeds, we measured the kinetics of fluorescence responses to voltage steps at room temperature and 37 °C. Activation kinetics were well modelled as a sum of two exponentials. At room temperature, ASAP4e was faster than ASAP4b in responding to depolarization, with fast activation kinetics of 2.6 ms vs 3.9 ms, accounting for 14% and 19% of the response amplitude, respectively (Supplementary Table 1). At 37 °C, ASAP4b and ASAP4e activation kinetics accelerated, with the fast component reaching similar values of 1.5 ms each (Supplementary Table 1)

To understand how well ASAP4b and ASAP4e can report voltage dynamics of mammalian neurons, we first tested responses in HEK293A cells to AP waveforms recorded from rat hippocampal neurons in culture. At room temperature, responses to APs of 2-ms full-width at half-maximum (FWHM) followed the rank order ASAP4b < ASAP3 < ASAP4e, with F_{AP}/F_{-70} values of 19%, 22%, and 23% respectively (Extended Data Fig. 5a). In response to 4-ms APs, which can be more easily compared to previously reported results[7], fluorescence changes were 26%, 29%, and 34%, respectively (Extended Data Fig. 5a). In contrast, upward Ace2N-mNeon[9] showed 8% or 10% responses to 2-ms or 4-ms APs, respectively. ASAP4b and ASAP4e were able to discern single spikes within 50- and 100-Hz bursts of AP waveforms (Fig. 1c, Extended Data Fig. 5b).

We also benchmarked ASAP4b and ASAP4e performance in detecting naturalistic spike bursts at 37 °C. We imposed voltage waveforms of 1–4 spikes recorded from mouse hippocampal pyramidal neurons *in vivo* (baseline V_m of −60 mV, AP FWHM of 1 ms) onto HEK293A cells by patch-clamp. Responses to single APs were 24%, 30%, and 41%, respectively for ASAP3, ASAP4b, and ASAP4e, and bursts of 2–4 spikes could easily be read by all three GEVIs (Extended Data Fig. 5c). For example, individual spikes within a triplet with 9.3-ms and 18.2-ms intervals were well discerned (Fig. 1d). ASAP4b and ASAP4e, but not ASAP3, showed a higher response to the second spike within bursts; this is expected from the slowly activating component in ASAP4b and ASAP4e (Supplementary Table 1).

Taken together, our measurements indicate that ASAP4b and ASAP4e have the largest fluorescence responses of any GEVIs described so far, both relative to baseline and in absolute brightness change per molecule, and for both slow steps and fast spikes (Table 1).

ASAP4 expression and performance in brain tissue.

To rapidly obtain evidence that positively tuned ASAPs function well in neurons *in vivo*, we performed two-photon imaging of ASAP4b in the axon termini of L2 neurons in the fruit fly visual system during visual stimulation. L2 neurons respond to increased luminance with hyperpolarization and to decreased luminance with depolarization. As expected, ASAP4b

responded oppositely to the negatively tuned indicator ASAP2f, by dimming upon a bright stimulus and brightening upon a dark stimulus (Extended Data Fig. 6). ASAP4b response amplitudes were ~2-fold higher than ASAP2f, and activation kinetics were slightly faster (Extended Data Fig. 6). These results verify that ASAP4b functions *in vivo*, and further confirm its two-photon compatibility and ability to reveal subcellular electrical activity.

We next examined ASAP4b and ASAP4e expression in cultured rat neurons, first omitting localization tags to assess the efficiency of membrane export without additional regulators. Based on the fraction of baseline ASAP fluorescence colocalized with the plasma membrane marker CrimsonRFP-CAAX[26], fluorescence of ASAP4b and ASAP4e was slightly less membrane-restricted than that of ASAP3 after 7 days of expression (Extended Data Fig. 7a,b). However, the degree of export is variable, such that fluorescence is nearly completely membrane-restricted in some neurons (Extended Data Fig. 7c).

To discern individual cells when performing voltage imaging in vivo, it is useful to somatically enrich GEVI signals[26]. We thus determined if ASAP4b-Kv and ASAP4e-Kv, fusions of ASAP4b and ASAP4e to the Kv2.1 proximal retention and clustering segment[27], expressed well in the mouse brain compared to ASAP3-Kv, whose performance has been well validated *in vivo*[6,28]. We expressed each GEVI in mouse dorsal striatum or hippocampus by adeno-associated virus (AAV)-mediated transduction. One month after transduction, all three GEVIs were well expressed at the plasma membrane (Extended Data Fig. 7d). Striatal medium spiny neurons or hippocampal somatostatin-positive (SST+) interneurons expressing ASAP4b-Kv or ASAP4e-Kv were at least 40% as bright as neurons expressing ASAP3 under one-photon illumination (Extended Data Fig. 7e,f). Given their relative F_{-70}/F_{max} values, this suggests ASAP4b-Kv and ASAP4e-Kv were at least as well expressed as ASAP3. We obtained similar results when comparing hippocampal pyramidal neurons expressing ASAP4b-Kv and ASAP3-Kv under two-photon illumination (Extended Data Fig. 7g). These results thus indicate that ASAP4b-Kv and ASAP4e-Kv express well *in vivo* relative to ASAP3-Kv.

To assess if performance in AP detection in cells is predictive of performance in mammalian brain tissue, we performed simultaneous patch-clamp electrophysiology and imaging of soma-targeted versions of ASAP3 and ASAP4e (ASAP3-Kv and ASAP4e-Kv) in acute hippocampal slices. Here, Kv is a proximal retention and clustering signal from Kv2.1 that we found to efficiently target GEVIs to somata *in vivo*[6,29]. Under one-photon illumination, response amplitudes and the ability to discern AP trains up to 50 Hz were similar between the two indicators (Extended Data Fig. 8a), as expected from their behavior in cultured cells. SNR values were also similar for firing rates between 10 and 50 Hz (Extended Data Fig. 8b). Under two-photon imaging, responses to APs were again similar up to 50 Hz (Extended Data Fig. 8c), as were SNR values (Extended Data Fig. 8d). Compared to the one-photon case, two-photon illumination produced larger response amplitudes (35%), as expected from less background fluorescence (Extended Data Fig. 8a,c). When applying current steps to evoke AP trains in place of individual current spikes, ASAP4b-Kv demonstrated larger responses and SNR than ASAP3-Kv (Extended Data Fig. 9a–c), although ASAP4b-Kv demonstrated a longer delay from electrical to fluorescence peaks (Extended Data Fig. 9c), reflecting its slower kinetics (Supplementary Table 1). The ISI distributions between

ASAP3-Kv and ASAP4b-Kv were very similar (Extended Data Fig. 9d), indicating both proteins had similar amounts of time for protein relaxation between APs, and that ASAP4b-Kv does not appreciably alter the propensity of the neuron to fire during current steps relative to ASAP3-Kv. These results indicate that the performance of ASAP4b-Kv initially characterized in HEK293 cells is well preserved in neurons in brain tissue.

To assist users in expressing ASAP-family GEVIs by AAV transduction, we tested several promoters and viral serotypes. For expression in all neurons, we found that the hSyn-ASAP-WPRE in AAV8 and AAV9 serotypes produced easily visible expression beginning 3 weeks post-injection. For cre dependent expression, CAG-DiO-ASAP-WPRE produced brighter cells but was toxic, while hSyn-DiO-ASAP-WPRE did not result in noticeable expression. EF1α-DiO-ASAP-WPRE in AAV8 or AAV9 produced steady bright expression beginning 3 weeks post-injection when coupled with a cre-expressing AAV giving excellent expression by 3-4 weeks post injection. We have been able to image mice repeatedly for more than 3 months with either the synapsin or EF1α promoter.

ASAP4e-Kv enables long activity recordings under one-photon illumination in the mouse brain.

While one-photon voltage imaging with ASAP-family GEVIs in the brain has not been reported previously, their higher molar brightness than opsin-only GEVIs, which have been used for *in vivo* one-photon imaging, suggests they should work as well. We expressed ASAP3-Kv, ASAP4b-Kv, or ASAP4e-Kv in SST+ interneurons of mice in the dorsal CA1 region of the hippocampus, and performed imaging through a deep window while mice were awake, head-fixed, and running. Illumination by a blue LED at power densities of 35–150 mW/mm^2, an order of magnitude less intense than previously used for one-photon opsin imaging[7], was sufficient for ASAP3-Kv, ASAP4b-Kv, or ASAP4e-Kv to reveal spikes with framerates of 400–1000 frames per s (fps) (Fig. 2a). Consistent with our *in vitro* observations, some ASAP4e-Kv traces showed photoactivation, so that signal intensity and apparent SNR were preserved for over 80 s of accumulated recording time. ASAP-family GEVIs thus allow extended one-photon voltage imaging in the brain, in contrast to opsin-only GEVIs where the intense illumination powers required (800–1600 mW/mm^2) limit recordings to ~12 s due to brain heating[7].

As some of the above experiments used interrupted bouts of illumination, we also compared photostability of ASAP3-Kv, ASAP4b-Kv, and ASAP4e-Kv *in vivo* under continuous illumination. ASAP3-Kv, ASAP4b-Kv, and ASAP4e-Kv showed $22 \pm 5\%$, $32 \pm 8\%$, and $0 \pm 10\%$ fluorescence loss (mean $\pm$ SEM of 4 neurons each), respectively, after 60 s of 100 mW/mm^2 illumination (Fig. 2b, Extended Data Fig. 10a). ASAP4e-Kv's exceptional mean photostability was again due to some cells exhibiting photoactivation. Photoactivation may have been recorded only in some cells due to different light doses applied while searching for cells, which we did not record.

We tested if ASAP4-family GEVIs could perform extended activity recordings in other cell types. At a power sufficient for detecting spiking activity (150 mW/mm^2), ASAP4b-Kv in hippocampal pyramidal neurons exhibited only 10% photobleaching after 30 s illumination (Extended Data Fig. 10b). At 50 mW/mm^2, ASAP4e-Kv in layer-1 cortical interneurons

exhibited minimal photobleaching after 45 s (Fig. 2c). These data show ASAP4-family GEVIs enable one-photon voltage imaging with high photostability in multiple neuronal types.

To quantify the ability of ASAP GEVIs to detect single APs with one-photon illumination, we employed a template-matching log-likelihood strategy based on log-likelihood probability calculations[30] and assuming Gaussian noise distributions (Fig. 3a,b, see methods). Briefly, putative APs for training were identified from optical spikes occurring selectively in the negative direction for ASAP3-Kv and in the positive direction for ASAP4e (Fig. 3a,b). As deflections in the incorrect direction are due to noise, this allowed the establishment of an amplitude threshold beyond which optical spikes in the correct direction are predominantly reporting APs. At least 10 of the largest of these spikes were chosen to serve as templates for the log-likelihood calculation. New template spikes were chosen for each trial, and if good templates were not available in a trial, then the templates from the same cell but a different trial were used. While this results in conservative detection, we wanted to be sure we did not have many false positives. The log-likelihood function itself exhibited a symmetric distribution with positive outliers; a threshold was set to identify these outliers as AP events (Fig. 3a,b). Using this algorithm, optical spike amplitudes (F_{event}/F_{rest}) averaged 10.2 % for ASAP3-Kv and 11.5 % for ASAP4e-Kv, and empirically measured SNR values averaged 2.8 and 2.3, respectively (Fig. 3c).

To determine if GEVIs can relate spike generation to subthreshold modulation in the same neurons, we also examined spike onset probability as a function of theta phase. Fluorescence traces were bandpass filtered from 6 to 11 Hz, then the Hilbert transform applied to obtain the instantaneous amplitude and phase, and a histogram of the theta phase values when spikes occurred was created. Both ASAP3-Kv and ASAP4e-Kv showed a preference for spiking near the peak of theta, which was set to 0 radians, although spikes can also be seen at other points in theta phase as well (Fig. 3d). Our results confirm findings from simultaneous whole-cell patch-clamping of SST+ interneurons and field electrode recordings in the mouse hippocampus[31].

Comparing voltage and calcium imaging for place cell detection *in vivo*.

ASAP-family GEVIs differ from the opsin-based GEVIs previously used for one-photon imaging in that they are also responsive under two-photon imaging. We also tested whether GEVIs could substitute for GECIs in activity imaging experiments performed with standard raster-scanning two-photon microscopes. We coexpressed GEVIs with the red GECI jRGECO1b[35] to simultaneously record voltage and calcium in CA1 pyramidal neurons as mice navigated a virtual reality environment to find hidden rewards (Fig. 4a,b). For this task, we chose ASAP4b-Kv as we desired to scan as many neurons as possible, and the higher molecular brightness at rest may be more useful for detecting multiple neurons over a large region, similar to the use case for jGCaMP7b[32]. With minimal modifications to a commercially available resonant-scanning two-photon microscope (Neurolabware), we were able to continuously image rectangular fields of view containing >50 cells at 989 fps for tens of minutes (Fig. 4c). To minimize power delivery and employ a commonly available imaging setup, we used one excitation laser at 940 nm at a minimum power capable of

detecting ASAP4b-Kv at baseline, and split green (ASAP4b-Kv) and red (jRGECO1b) signals to separate detectors.

Applying an analysis pipeline previously developed for calcium imaging to ASAP4b-Kv fluorescence (see Methods), we identified a large population of place cells (~30% of cells with significant spatial information). As expected from calcium imaging and extracellular voltage recordings, ASAP4b-Kv place cells tiled the environment with their place fields (Fig. 4d–g). Calcium and voltage activity rate maps were largely consistent in cells with strong co-expression, but ASAP4b-Kv signals clearly demonstrated higher temporal resolution and better ability to discern closely spaced spikes (Fig. 4d,g). Thus, using a standard commercial two-photon microscope system designed for imaging GECIs, we were able to record populations of place cells in the hippocampus by imaging ASAP4b-Kv. Additionally, the signals were large and robust enough that a standard calcium imaging data processing pipeline was able to pull out place cell tiling in the green ASAP4b-Kv channel that matched the red jRGECO1b channel (Fig. 4g).

Extended simultaneous imaging of calcium and voltage *in vivo* with ASAP4e-Kv.

Genetically encoded calcium indicators (GECIs) are widely used to reveal neuronal activity *in vivo*, but the slow kinetics of these indicators and of calcium transients themselves prevents the reliable reconstruction of spike patterns from GECI signals[33]. A GEVI that could detect APs using standard two-photon scanning methods may allow more accurate assessment of spiking activity without requiring expensive equipment upgrades. We thus explored whether ASAP4's extended decay kinetics (Supplementary Table 1) could allow it to report APs at a sampling rate of 100 fps, only several-fold faster than standard GECI imaging conditions.

We co-expressed the dimmer but more responsive ASAP4e-Kv and the red GECI jRGECO1a in layer 2/3 of mouse cortex, then performed imaging with 1000-nm two-photon excitation in awake, head-fixed animals. We chose jRGECO1a to co-image with ASAP4 as it was the red GECI with the largest per-AP responses, and indeed detects APs in vivo better than GCaMP6f[35]. We imaged 13 spontaneously active neurons in one animal, acquiring 128×128-voxel frames at 15 to 99 fps. ASAP4e-Kv photostability was excellent; in 100-s continuous recordings at 99 fps, 91% of beginning fluorescence was retained (Fig. 5a, Supplementary Video 1). Despite the 1000-nm excitation being non-optimal for ASAP, we observed that each GECI transient was temporally preceded by ASAP4e-Kv signals (Fig. 5a, Supplementary Video 1). Indeed, these ASAP4e-Kv signals extended across multiple frames, indicating spike bursts (Fig. 5b). In addition, several clear ASAP4e-Kv transients were associated with small changes in jRGECO1a fluorescence that were not clearly distinguishable from noise (Fig. 5a,b). As jRGECO1a has superior single-AP responses in vitro and AP detection in vivo to GCaMP6f[34,35], our findings suggest that ASAP4e-Kv can detect APs with higher reliability than widely used GECIs under standard two-photon scanning conditions. This is consistent with a recent report that only a minority of single APs are detected by GCaMP6f under standard two-photon population imaging conditions[33]. In addition, our findings show that ASAP4e-Kv can be used to detect APs at acquisition speeds achievable by raster-scanning two-photon microscopes.

DISCUSSION

In this study, we introduce two positively tuned and highly responsive GEVIs, ASAP4b and ASAP4e, with improved photostability over previous ASAP-family GEVIs under one-photon illumination. We demonstrate the ability of ASAP4b and ASAP4e to detect spiking activity in single trials *in vivo* by both one-photon and two-photon imaging. In particular, we show that ASAP4e can be used to detect APs in the mammalian brain *in vivo* for minutes of continuous one-photon or two-photon illumination using commonly available epifluorescence or raster-scanning microscopes. This ability opens up new uses for ASAP-family GEVIs. For example, monitoring the subthreshold and spiking activity of multiple cells can be used to determine how oscillations relate to spiking activity in different neurons within a local network, and whether such relationships are modulated by stimuli or experience.

We demonstrate simultaneous single-cell voltage and calcium imaging by two-photon microscopy of ASAP4e and ASAP4b with jRGECO1a, showing that ASAP4 variants can be used alongside red GECIs to image voltage on a standard galvanometric two-photon imaging setup, even at frame rates as low as 99 Hz. We also find that a standard calcium imaging pipeline[36] can be applied to voltage images to map place cells. This should further ease the transition from calcium imaging to voltage imaging for neuroscience laboratories.

The results of ASAP4e-Kv and jRGECO1a co-imaging add to a recent report that GCaMP6f does not capture all spiking activity in vivo standard two-photon imaging conditions[33]. Due to its wide usage and the familiarity many researchers have with its performance, GCaMP6f serves as a convenient reference point for AP detection. Within the last year, GECIs that further improve single-AP sensitivity in vitro and activity detection in vivo have been reported in preprint[37]. Comparisons between these new GECIs and ASAP4e-Kv will be informative, although more difficult as they are in the same spectral class and thus cannot be imaged simultaneously. However, the slow off-kinetics of calcium after APs (>60 ms in cortical pyramidal neuron cell bodies), which are inherent characteristics of calcium transients themselves[38], are expected to continue to impede the ability of GECIs to resolve APs within spike bursts or trains.

Photon shot noise is related to the square root of signal intensity, which includes background fluorescence. Thus, in shot noise-limited imaging conditions, the lower baseline brightness of ASAP4e-Kv should be preferable to the higher baseline of ASAP3-Kv, as it should produce less out-of-focus background. However, we observe ASAP3-Kv and ASAP4e-Kv to have similar per-cell SNRs for spikes. There are two possible explanations. First, simulations suggest that GEVI responses should exceed 40% F/F and cell density should exceed 200 cells/mm^2 before lower baseline fluorescence can noticeably improve SNR[9]. Neither condition was met in our experiments. In addition, all of our fluorescence signals exhibited Gaussian noise statistics, not the Poisson statistics expected for the shot noise-limited regime, suggesting noise from other sources, such as electronics or motion, dominate.

Future improvements to ASAP-family GEVIs could further improve photostability either directly or by reducing illumination requirements. In response to steady-state voltages from −70 to +30 mV, ASAP4e operates from 20% to 57% of the maximum brightness of its GFP fluorophore. Sharpening the F-V curve to further decrease fluorescence at −70 mV or increase fluorescence at +30 mV will produce larger responses. Accelerating activation kinetics will allow for more of the already substantial steady-state fluorescence range (210% for ASAP4e) to be sampled during APs. Such optimizations would yield higher SNRs while maintaining sampling rate or illumination power, or could allow faster sampling or lower powers at the same SNR, thereby increasing reliability of event detection or duration of recording.

In summary, we perform voltage imaging using ASAP4-family GEVIs on existing one-photon and two-photon equipment previously developed for imaging GECIs, demonstrating that voltage imaging is within the technical abilities of a large number of neuroscience laboratories. GEVI imaging should be widely applicable for recording neuronal spiking activity with higher temporal precision than possible with calcium imaging, or for relating spiking activities to subthreshold dynamics.

METHODS

Plasmid Construction.

For transfection into HEK293-Kir2.1 Cells for electrical screening, the parent ASAP2f L146G S147T R414Q was subcloned into pcDNA3.1 with a CMV enhancer and promoter and bGH poly(A) signal. All plasmids were made by standard molecular biology techniques with all cloned fragments confirmed by sequencing (Sequetech). PCR reactions were carried out to generate PCR product libraries using standard PCR techniques, which were used to directly transfect HEK293-Kir2.1 cells with the linear product using lipofectamine 3000 (Thermo Fisher Scientific). For patch clamp characterization in HEK293A cells, all voltage indicators were subcloned into a pcDNA3.1/Puro- CAG vector between NheI and HindIII sites[20].

For in vitro characterization in cultured neurons, acute hippocampal slice and in vivo hippocampal imaging, ASAP variants were subcloned into pAAV.hSyn.WPRE. These were then midi-prepped and packaged into adeno-associated virus 8 (AAV8) by the Neuroscience Gene Vector and Virus Core of Stanford University. For somatic targeting in acute slice and in vivo, the C-terminus of ASAP4 variants was attached to the C-terminal cytoplasmic segment of the Kv2.1 potassium channel[27], that we previously used to restrict ASAP3 to the soma, axon and proximal dendrites[6]. For EF1α-driven ASAP expression, viral constructs were generated by modifying published methods[39] using GateWay recombination and Gibson assembly, and produced in-house as previously described[6,40]. These were then packaged into AAV8 capsids by the Neuroscience Gene Vector and Virus Core at Stanford University.

For quantification of membrane trafficking, ASAP variants (ASAP3 or ASAP4b or ASAP4e), internal ribosome-entry site (IRES), and Crimson-CAAX[26] were assembled into Lenti-DIO-EF1α backbone vector (Addgene #170327) between AscI and NheI sites using

HiFi DNA Assembly Master Mix (New England Biolabs). All constructs were confirmed by whole plasmid sequencing (Primordium labs).

Cultured Cell Lines.

All cell lines were maintained in a humidified incubator at 37°C with 5% CO_2. For electrical screening the previously described HEK293-Kir2.1 cell line[41] was maintained in high-glucose DMEM (Thermo Fisher Scientific), 5% fetal-bovine serum (FBS; Gemini bio), 2 mM L-glutamine (Gemini bio), and 500 μg/mL geneticin (Thermo Fisher Scientific). For patch-clamp recordings to measure ASAP responsivity and kinetics, HEK293A cells were cultured in high-glucose DMEM with 5% FBS and 2 mM L-glutamine.

Cultured Neurons.

Hippocampal neurons were isolated from embryonic day 18 Sprague Dawley rat embryos of both sexes. Procedures were carried out in compliance with the rules of the Stanford University Administrative Panel on Laboratory Animal Care.

Viruses.

AAV9-CamKII-Cre was obtained from the Penn Vector Core. AAV1-Syn-NES-jRGECO1a, 1x10^11 vg/mL, Addgene #100854, and AAV1-syn-NES-jRGECO1b-WPRE-SV40, AddGene #100857, were ordered from Addgene. All ASAP viruses were produced by the Stanford Neuroscience Gene Vector and Virus Core facility, and by the lab of Sui Wang at Stanford University.

For the acute slice brightness comparisons, viruses were diluted in phosphate-buffered saline (PBS) until the following titers were reached: AAV9-CamKII-cre at a titer of 5.6x10^9 vg/mL, and all three ASAP viruses at a titer of 3.45x10^11 vg/mL. For the two-photon imaging while patch clamping evoked spikes in hippocampal slice work, AAV8-syn-ASAP3/4b-Kv was injected at a titer between 1.21x10^12 and 5x10^12 vg/mL, and AAV1-syn-jrGECO1b was injected at a titer between 1.3x10^12 and 5x10^12 vg/mL, but we were not able to image the jRGECO1b well, so it was excluded from the analysis. For the one-photon imaging of patch clamping in hippocampal slice and evoking spikes, AAV8-syn-ASAP4b-Kv and AAV8-syn-ASAP3-Kv were injected at titers approximately between 1x10^12 and 1x10^13 vg/mL. For the in vivo two-photon imaging of ASAP4e and jRGECO1a in V1, AAV8-Syn-ASAP4e-Kv at a titer of 4.66x10^11 vg/mL was co-injected with AAV1-Syn-NES-jRGECO1a at a titer of approximately 1x10^11 vg/mL. For the in vivo one-photon imaging of hippocampus during running, either AAV8-ef1α-DiO-ASAP3-Kv at a titer of 2.35x10^12 vg/mL, AAV8-ef1α-DiO-ASAP4b-Kv at a titer of 2.36x10^12 vg/mL, or AAV8-ef1α-DiO-ASAP4e-Kv at a titer of 3.45x10^11 vg/mL was injected. For the in vivo two-photon imaging of the hippocampus during a spatial navigation task, AAV8-syn-ASAP4b-Kv at a titer of 1.17×10^12 vg/mL was co-injected with AAV1-syn-NES-jRGECO1b-WPRE-SV40 at a titer of 1.3x10^13.

Lentiviruses were produced for the membrane trafficking quantification experiment by a previously described method[42]. Briefly, low-passage-number HEK293T cells (ATCC CRL-3216) were plated onto 15-cm dishes (Corning TCA-430599) in DMEM (Gibco

31-053-036) supplemented with 10% FBS, 2 mM L-Glutamine and 1% Penicillin/ Streptomycin (DMEM10). When HEK293T cells reached 80% confluency, the medium was exchanged to a serum-free DMEM. After 1h, the cells were transfected using polyethylenimine (PEI; Polysciences 23966) with 15.5 μg of the vector plasmid (pLenti-DIO-EF1α-ASAPx-IRES-Crimson-CAAX), 10 μg of the second-generation packaging plasmid psPAX2 (Addgene #12260), and 4.5 μg of viral entry protein VSV-G plasmid pMD2.G (Addgene #12259). The three plasmid DNAs were mixed into 1.35 mL of serum-free DMEM and 40 μL of 1 mg/mL PEI was added at the end. The mixture was incubated at room temperature for 10 min and added dropwise to the culture. After 4 h, the medium was exchanged back to 18 mL of DMEM10. The supernatant was harvested at 36 h post-transfection and kept at 4 °C. Then, 18 ml of DMEM10 was added to the cells and incubated for another 24 h. At 60 h post-transfection, the supernatant was harvested again and combined with the first batch of supernatant, centrifuged for 5 min at 1500 g, and filtered through a 0.45-μm syringe filter (EMD Millipore SLHVR33RB). Next, 12 mL Lenti-X concentrator (Takara Bio #631232) was added to the supernatant and incubated in 4 °C for 1 h. Viruses were centrifuged for 45 min at 1500 g and dissolved in PBS. Titer of the lentiviruses were measured with Lenti-X GoStix (Clontech #631244) kit after 1:100 dilution. The viral particles were aliquoted, and stored at −80 °C for neuronal transduction.

Animals.

For the one-photon acute slice brightness comparisons, two-photon acute slice patch clamping experiments and in two-photon in vivo imaging experiments, adult male and female wild-type C57BL/6 were used. All mice were housed in standard conditions (up to five animals per cage, 12-hour light/dark cycles with the light on at 7 a.m., with water and food ad libitum). Day-18 Sprague Dawley rat embryos were used for hippocampal tissue for neuronal culture. All protocols were approved by the Stanford Institutional Animal Use and Care Committee.

For the *in vivo* fly imaging, ASAP4b was cloned into the pJFRC7-20XUAS vector[43] using standard molecular cloning methods (GenScript Biotech), and then inserted into the attP40 phiC31 landing site by injection of fertilized embryos (BestGene). We used the cell type-specific driver 21D-GAL4[44] to express ASAP2f and ASAP4b in L2 cells. We imaged the axon terminals of L2 cells in its medulla layer M2 arbors. The genotypes of the imaged flies in Extended Data Fig. 6 were: L2>>ASAP2f: +; UAS-ASAP2f/+; 21D-Gal4/+. L2>>ASAP4b: yw/+; UAS-ASAP4b/+; 21D-GAL4/+.

In vivo one-photon imaging experiments were conducted at the University of California at Los Angeles (UCLA), where adult (11–23 week old) SST-IRES-cre knock-in adult male and female mice were used for all experiments. All animals were group housed (2–5 per cage) on a 12 h light/dark cycle. All experimental protocols were approved by the Chancellor's Animal Research Committee of UCLA in accordance with NIH guidelines.

Animals used in acute slice one-photon patch clamping experiments were male and female wild-type mice aged 20–40 days. All mice used were maintained on a 12-h light/dark cycle, with food and water available ad libitum and in accordance with the Institutional Animal Care and Use Committee of Columbia University.

For the co-imaging of ASAP4e and jRGECO1a in V1, all animal experiments were conducted according to the National Institutes of Health guidelines for animal research. Procedures and protocols on mice were approved by the Animal Care and Use Committee at the University of California, Berkeley.

Cell screening.

HEK293-Kir2.1 cells were plated in 384-well plates (Grace Bio-Labs) on conductive glass slides (Sigma-Aldrich). Cells were transfected with PCR-generated libraries in 384-well plates with Lipofectamine 3000 (~100 ng DNA, 0.4 μL p3000 reagent, 0.4 μL Lipofectamine) followed by a media change 4–5 hours later, with imaging done 2 days post-transfection in Hank's Balanced Salt solution (HBSS; Cytiva) buffered with 10 mM HEPES (Thermo Fisher Scientific). Cells were imaged at room temperature on an IX81 inverted microscope fitted with a 20× 0.75-numerical aperture (NA) objective (Olympus). A 120-W Mercury vapor short arc lamp (X-Cite 120PC, Exfo) served as the excitation light source. The filter cube set consisted of a 480/40-nm excitation filter and a 503-nm long pass emission filter. ASAP libraries were screened at room temperature with the operator locating the best field of view and focusing on the cells. A single field of view was imaged for a total of 5 s, with a 10-μs 150-V electroporating square pulse applied near the 3-s mark as previously described[6]. Fluorescence was recorded at 100 Hz (10-ms exposure per frame) by an ORCA Flash4.0 V2 CMOS camera (Hamamatsu C11440–22CA) with pixel binning set to 4×4. Mutants were screened at least three times.

Whole cell patch clamping and imaging of HEK293A cells.

Patch-clamp experiments were mainly done as previously described[6]. Cells were transfected with pcDNA3.1/Puro-CAG-based plasmids expressing each GEVI using Lipofectamine 3000 (400 ng DNA, 0.8 μL P3000 reagent, 0.8 μL Lipofectamine) per manufacturer's recommended instructions. After plating the cells on 12 mm glass coverslips (Carolina Biological), the cells were patch clamped 24 hours after transfection. Signals were recorded in voltage-clamp mode with a Multiclamp 700B amplifier and using pClamp software (Molecular Devices). Fluorophores were illuminated at ~4.3 mW/mm^2 power density at the sample plane with a blue LED (Prizmatix UHP-Mic-LED-460) passed through a 484/15-nm excitation filter and focused on the sample through a 40× 1.3-NA oil-immersion objective (Zeiss). Emitted fluorescence passed through a 525/50-nm emission filter and was captured by an iXon 860 electron-multiplied charge-coupled device camera (Oxford Instruments) cooled to −80 °C. For all experiments fluorescence traces were corrected for photobleaching by dividing the recorded signal by a mono-exponential fit to the data.

To characterize steady-state fluorescence responses, cells were voltage-clamped at a holding potential of −70 mV, then voltage steps of 1 s duration were imposed at −120, −100, −80, −60, −40, −20, 0, 30, 50, 70, 90, and 120mV. To obtain complete fluorescence–voltage (F–V) curves, the above steps plus additional ones at −200, −180, −160, −140, and 120mV were imposed. When voltage-clamp could not be imposed on some cells at the highest potentials, that step was excluded from data analysis. A scaled action potential waveform (FWHM 3.5 ms, −70mV to +30mV) recorded from a cultured hippocampal neuron was included before each step to estimate the fluorescence change of the indicators to action

potential waveform. To estimate per-molecule brightness, we assume the chromophore with the cpGFP domain of each ASAP variant has similar molar brightness in its deprotonated 490 nm-absorbing state. This assumption is based on the observation GCaMP GECIs, which have the same chromophore, show similar per-molecule brightness to EGFP upon 490-nm excitation when fully calcium-saturated and deprotonated[34], despite the cpGFP domain of GcaMPs presenting a different environment around the group ring than the EGFP domain. That is, the identical chromophores in cpGFP and EGFP exhibit similar brightness when deprotonated, despite different chromophore environments near the phenotpye group, and thus we assume the deprotonated states of ASAP variants will be similarly bright to each other. A relative measure of population brightness at rest for equivalent numbers of molecules expressed (mF_0) is then given by $F_{-70}/F_{\max}$, the brightness at –70mV relative to maximum fluorescence across all voltages. We obtained F-V readings across a wide-enough V range to obtain asymptotic maximum F values.

To characterize kinetics of ASAP indicators at both room temperature and 37 °C, images were acquired at 2.5 kHz from an area cropped down to 64×64 pixels and further binned to comprise only 8×8 pixels. Fluorescence was quantified by averaging pixels with signal change in the corresponding cell shape after subtracting by the background pixels. Command voltage steps were applied for 1 s, and a double exponential or single exponential fit was applied to a 60-ms interval from the starting point of the onset and offset of voltage steps using MATLAB software (MathWorks). To characterize GEVIs on simulated AP burst waveforms (2 and 4 ms at FWHM) at room temperature, images were acquired at 1000 Hz from a 64×64-pixel FOV, then binned using 4×4 pixel binning. To characterize ASAP variants on square pulses (1, 2, and 4 ms, –70mV to +30mV) and AP burst waveforms (FWHM 1.0 ms) at 37 °C, images were acquired at 2500 Hz from a 64×64-pixel FOV, then 8×8 binning was applied.

One-photon excitation and emission spectra measurements.

HEK293-Kir2.1 cells were cultured as described above until 70–80% confluency, then transfected using Lipofectamine 3000 (Thermo Fisher) with pCAG-ASAP4.2-F413S construct. Two days post-transfection, approximately 1×10^5 cells were replated in a 96-well plate in PBS. The excitation spectra from 300 to 530 nm, upon emission at 550 nm with a bandwidth of 10 nm, and the emission spectra from 500 to 850 nm, upon excitation at 480 nm with a bandwidth of 10 nm were obtained in an Infinite M1000 Pro microplate reader (Tecan). Spectra were averaged over 4 wells and normalized to its peak value.

Primary neuronal culture and transfection.

Hippocampal neurons were isolated from embryonic day 18 (E18) Sprague Dawley (SD) rat embryos by dissociating them in RPMI medium containing 5 units/mL papain (Worthington Biochemical) and 0.005% DNase I at 37 °C and 5% CO2 in air. Neurons were plated on washed 12-mm No.1 glass coverslips pre-coated overnight with > 300-kDa poly-D-lysine hydrobromide (Sigma-Aldrich). Cells were plated for several hours in Neurobasal media with 10% FBS (Gemini bio), 2 mM GlutaMAX (Thermo Fisher Scientific), and B27 supplement (Thermo Fisher Scientific), then the media was replaced with Neurobasal with 1% FBS, 2 mM GlutaMAX, and B27. Half of the media was replaced every 3–4 days with

fresh media without FBS. 5-Fluoro-2'-deoxyuridine (Sigma-Aldrich) was typically added at a final concentration of 16 μM at 7–9 DIV to limit glial growth. Hippocampal neurons were transfected at 9–11 DIV with 500 ng total DNA including 100–300 ng of indicator DNA and 1 μL Lipofectamine 2000 (Thermo Fisher Scientific) in 200 μL Neurobasal with 2 mM GlutaMax.

Cortical neurons from E18 rat embryos were dissected as previously described[6]. Briefly, 1×10^5 dissociated rat cortical neurons were plated in each well of 24-well glass bottom plates (Cellvis; P24-1.5H-N) that was coated with >300-kDa poly-D-lysine hydrobromide (Sigma-Aldrich #P1024). The cells were incubated for 1-day in Neurobasal media with 10% FBS, 2 mM GlutaMAX, and B27 supplement (Thermo Fisher Scientific), then the media were replaced with the same media but with 1% FBS. A half of the media was then replaced every 3 days with fresh Neurobasal media without FBS. 5-Fluoro-2'-deoxyuridine (Sigma-Aldrich #F0503) was typically added at a final concentration of 16 mM at DIV 4 to limit excessive non-neuronal cell growth. On DIV 7, the cortical neurons were infected with Lenti-DIO-EF1α-ASAPx-IRES-Crimson-CAAX virus, and then transfected with pCAG-iCre (Addgene #89573) plasmid on DIV 8, using Lipofectamine 2000 (Thermo Fisher Scientific).

High resolution cultured hippocampal neuron imaging.

Cultured hippocampal neurons were transfected at 9–11 DIV via Lipofectamine 3000 (Thermo Fisher Scientific) with pAAV-hSyn-ASAPx-WPRE and pAAV-hSyn-Ace2-D92N-E199V-mNeon-ST-WPRE (upward Ace2N-mNeon) variants. Cells were imaged at 12–20 DIV on an inverted confocal microscope (Zeiss Axiovert 200M) with a 40× 1.2-NA objective (Zeiss). ASAPs and upward Ace2N-mNeon were excited by a 120-W Mercury vapor short arc lamp (X-Cite 120PC, Exfo) set to 12% maximum output and passed through a 488/30-nm filters, and fluorescence was collected via 531/40-nm filters. Images were taken using an ORCA Flash4.0 V2 C11440-22CA CMOS camera (Hamamatsu) with Micro-manager software. Exposure time was 1 s per frame, with frames collected as 2048×2048 16-bit images.

One-photon photobleaching in HEK293-Kir2.1 cells.

HEK293-Kir2.1 cells were plated and cultured on a 60-mm culture dish (CellTreat) by using the same culture condition described above. At approximately 80% confluency, the cells in each dish were transfected with 4 μg of plasmid expressing ASAP3, ASAP4b, ASAP4e, or ncpASAP4b from a CMV promoter, and Lipofectamine 3000 per manufacturer protocols (8 μL of P3000 and 8 μL Lipofectamine in OptiMEM, all from Thermo Fisher Scientific). One day after transfection, cells were dissociated with 0.25% trypsin 0.53 mM EDTA solution (Gemini Bio) and replated onto 29mm-diameter glass-bottom dishes with a 20 mm-diameter #1.5 cover glass (CellVis). The next day, the media was replaced to HBSS containing 10 mM HEPES (Thermo Fisher Scientific). The transfected cells were then imaged under an Axiovert 200M microscope (Zeiss) using a 40× 1.2-NA water-immersion objective (Zeiss C-Apochromat). Illumination was provided with a 453-nm LED via a liquid light guide (Prizmatix UHP-F-3-455 and LLG-3) and filtered through a green fluorescence filter set (Zeiss BP 450-490, FT 510, BP 515-565). By controlling the LED's current level and by

using a neutral density filter with optical density of 1 (10% transmittance), five different excitation power levels could be used for the photobleaching experiments. Emission was then acquired with a Flash 4.0LT+ CMOS camera (Hamamatsu C11440) at a framerate of 5 fps for 5 min of continuous illumination. The camera was controlled by μManager[45] and images saved as TIFF stacks. The TIFF stacks were analyzed in NIH Fiji[46] by manually selecting cellular ROIs as well as a dark background ROI for each FOV and measuring mean intensities. Background-substrated intensities were calculated and normalized to the initial value in Excel (Microsoft).

Two-photon photobleaching and excitation spectra measurements in HEK293-Kir2.1 cells.

HEK293-Kir2.1 cells were cultured as described above and then plated on 12-mm diameter coverslips (0.13–0.17 mm thickness, Carolina Biological) coated with poly-D-lysine (MP Biomedicals). The cells were transiently transfected at 60–80% confluency with 200–300 ng of expression plasmid expressing GEVIs from a CMV promoter and Lipofectamine 3000 per manufacturer protocols (0.8 μL of P3000 and 0.8 μL Lipofectamine in OptiMEM). The transfected cells were imaged 1–3 days post-transfection. During imaging, cells were bathed in HBSS supplemented with 10 mM HEPES. For experiments without recovery, cells were imaged using resonant galvonometer scanning (8-kHz line scan rate) on a Bruker Ultima system with a 20× 1.0 NA water immersion objective (Leica). The excitation laser (Spectra-Physics) was tuned to 920 nm, and signals were collected by a GaAsP-type photomultiplier tubes after a 525/50-nm filter, with a frame rate of 75 Hz. The resolution was 800×200 pixels with 0.65 μm spacing. For experiments with recovery, custom-built two-photon microscope system using a tunable two-photon laser (Spectra-Physics InSight X3) was modulated with a Pockel's cell (Conoptics 350-80). The laser was directed with a 12.0-kHz resonant scanner[47] and focused through a 40× 0.8-NA objective (Nikon). Cells were imaged under 930-nm light for ASAP4b and ASAP4e, or 940-nm light for ASAP3 and ncpASAP4b. Data were collected by a photomultiplier tube (Hamamatsu H10770PA-40), after being filtered for green light (Chroma ET525/50M).

Membrane trafficking quantification in cultured rat neurons.

Cortical neurons transduced with relevant Lentivirus as described above were imaged at DIV 15 (7 days after iCre transfection) in imaging solution (HBSS with 2 mM GlutaMAX, 1 mM sodium pyruvate, and 10 mM HEPES pH 7.4). As a membrane-localized reference channel, Crimson RFP[26] with a C-terminal farnesylation motif (CAAX) for membrane targeting was co-expressed with an ASAP variant via IRES. The epifluorescence from the cells were imaged on an Axiovert 200M inverted microscope with a 40x 1.2-NA water-immersion objective (Zeiss) and an X-Cite 120 metal-halide lamp (Exfo) as the excitation light source. For ASAP, excitation and emission filters were BP450-490 and BP515-565 (Zeiss). For Crimson, excitation and emission filters were HQ535/50m and HQ625/60m (Chroma). For each cell, 15 focal planes spaced 1 μm apart were captured by a Flash4.0LT+ camera using μManager. To quantify membrane localization, a custom-written MATLAB (MathWorks) code was used. Membrane masks of the neurons were generated by applying the graythresh function on Sobel-filtered red channel images. The soma masks were manually selected using the roipoly function on red channel images. Then the two masks were applied to

background-subtracted green channel images to obtain the membrane fluorescence and the soma fluorescence of the ASAP reporter. The total fluorescence is the sum of the two.

Two-photon in vivo imaging of *Drosophila*.

Flies were mounted, dissected to expose the brain, perfused with a saline-sugar solution, and imaged for up to 1 h, as previously described[12,48]. Neurons were excited at 920 nm with 5–15 mW of total power, and photons were collected with a 525/50-nm filter. Data was collected at 82.4 frames per s with 200×20-pixel frames using a 15× digital zoom, using bidirectional scanning. We used a Leica TCS SP5 II two-photon microscope with a Leica HCX APO 20× 1.0-NA water immersion objective (Leica) and a pre-compensated Chameleon Vision II femtosecond laser (Coherent, Inc.).

Visual stimuli were generated with custom-written software using MATLAB (MathWorks) and presented using the blue LED of a DLP Lightcrafter 4500 (Texas Instruments) projector in Pattern Sequence mode. The stimulus was refreshed at 300 Hz and utilized 6 bits/pixel, allowing for 64 distinct luminance values. The stimulus was projected onto a 9×9-cm rear-projection screen positioned approximately 8 cm anterior to the fly that spanned approximately 70° of the fly's visual field horizontally and 40° vertically. A small square was also simultaneously projected onto a photodiode (Thorlabs, SM05PD1A) configured in a reversed-biased circuit. The stimulus was filtered with a 482/18-nm bandpass filter so that it could not be detected by the microscope PMTs. The radiance at 482 nm was approximately 78 mW sr^{-1} m^{-2}.

The Imaging and the visual stimulus presentation were synchronized using triggering functions provided by the LAS AF Live Data Mode software (Leica) as well as the signal from the photodiode directly capturing projector output. A Data Acquisition Device (NI DAQ USB-6211, National Instruments) connected to the computer used for stimulus generation was used to acquire the photodiode signal, generate a trigger signal at the beginning of stimulus presentation, and acquire the trigger produced by the LAS software at the start of each imaging frame. This allowed the imaging and the stimulus presentation to initialize in a coordinated manner and ensured that stimulus presentation details were saved together with imaging frame timings (in MATLAB .mat files) to be used in subsequent processing. Data was acquired on the DAQ at 5000 Hz.

The visual stimuli used were 300-ms search stimuli: alternating full contrast light and dark flashes, each 300 ms in duration, were presented at the center of the otherwise dark screen. The stimulus was such that from the perspective of the fly, the flashing region was 8° from each edge of the screen. In subsequent analysis, the responses to this stimulus were used to select ROIs with receptive fields located at the center of the screen instead of at the edges. This stimulus was presented for 5000 imaging frames (61 s) per field of view. Single 20-ms light and dark flashes, with 500-ms of gray between the flashes, were presented over the entire screen. The light and dark flashes were randomly chosen at each presentation. The Weber contrast of the flashes relative to the gray was 1. This stimulus was presented for 10,000 imaging frames (122 s) per field of view.

The acquired time series was saved as .lif files and read into MATLAB using Bio-Formats (Open Microscopy Environment). Each time series was aligned in x and y coordinates by maximizing the cross-correlation in Fourier space of each image with a reference image (the average of the first 30 images in the time series). For each time series, ROIs around individual arbors were selected by thresholding the series-averaged image with a value that generates appropriate ROIs, and then splitting any thresholded ROIs consisting of merged cells and/or adding ROIs that were missed by the thresholding. The fluorescence response for each time series was calculated after subtracting the background intensity and correcting for bleaching as previously described [12,48]. Time series with uncorrected movement, which was apparent as irregular spikes or steps in the F/F traces that were coordinated across ROIs, were discarded. The stimulus-locked average response was computed for each ROI by reassigning the timing of each imaging frame to be relative to the stimulus transitions (gray to light or gray to dark) and then computing a simple moving average. The averaging window was 8.33 ms and the shift was 8.33 ms, which effectively resampled our data from 82.4 to 120 fps.

As the screen on which the stimulus was presented did not span the fly's entire visual field, only a subset of imaged ROIs experienced the stimulus across approximately the entire extent of their spatial receptive fields. These ROIs were identified based on having a response of the appropriate sign to the 300-ms search stimulus. ROIs lacking a response to these stimuli or having one of the opposite sign were not considered further. The peak response to each flash (peak F/F) was the F/F value farthest from zero in the expected direction of the initial response (depolarization or hyperpolarization). The time to peak (t_{peak}) was the time at which this peak response occurred, relative to the start of the light or dark flash. Pairwise Student's t-tests were performed.

Acute slice brightness comparisons.

Viruses were diluted with PBS until the following titers were reached: 3.5×10^{11} genome copies (GC) per mL for AAV8-EF1α-fLex-ASAP3/4.4/4.5 and 5.6×10^9 GC/mL for AAV9-CamkII-cre, which was obtained from the uPenn viral core (Addgene plasmid #105558). Mice were injected at postnatal ages 40–56 days. Each mouse was injected with 950–1000 nL at a flow rate of 200 nL/min. Acute slices were obtained 28–36 days post-injection. Injections were performed at the following coordinates relative to Bregma: AP: +1.2 mm; ML: –2 mm; DV: –3.2 to –2 mm, placing them into the dorsal striatum. Light was delivered to and received from the samples via a GFP filter cube (Chroma U-N41017 EN), through a 40x water immersion objective (Olympus LUMPlanFL 40×). To control for fluctuations in illumination intensity, videos of 50 frames were recorded at 33 Hz with a 30-ms exposure time, and the average taken. Imaging was done with the Orca Flash4.0 LT camera. ROIs for the cells were drawn in NIH Fiji, taking the mean pixel value within the ROI. Background was determined as the tissue near the cell without any cell debris present, and the mean was taken and subtracted out to give the final brightness value for a cell.

Simultaneous one-photon imaging and electrophysiology in hippocampal slice.

Mice aged 20–40 days were injected with AAV expressing ASAP3-Kv or ASAP4b-Kv. 4–7 days post-injection, animals were anesthetized with 5% isoflurane and acute coronal

slices were prepared as previously described[49]. After achieving whole-cell recording configuration, APS were evoked in current clamp mode using 1-ms injections of 1 nA. Images were simultaneously recorded at ~1000 frames per second using a blue LED light source (coolLED pe300) and a photometrics prime-95B camera (Teledyne Photometrics) with a 40×W 0.8-NA objective (Olympus LUMPLFLN).

Simultaneous two-photon imaging and electrophysiology in hippocampal slice.

Mice of 28–60 days postnatal age were anesthetized with either ketamine/xylazine or isofluorane, then injected with a 1-μL mixture of AAV8-syn-ASAP3/b-Kv-WPRE and AAV1-syn-jRGECO1b-WPRE into the right hippocampus. Final concentrations were between 1.21×10^{12} and 5×10^{12} GC/mL for AAV8-syn-ASAP3/b-Kv-WPRE and between 1.3×10^{12} and 5×10^{12} GC/mL for AAV1-syn-jRGECO1b-WPRE. The mixture was injected via a glass micropipette (VWR) pulled with a long narrow tip (size ~10–20 μm) by a micropipette puller (Sutter Instrument) at a rate of 100 nL/min at the following coordinates from bregma: AP: −1.5 mm. ML: −1.5mm. DV: −1.5 to −1.3mm. The pipette was gently withdrawn 5 min after the end of infusion and the scalp was sutured.

Coronal brain slices (300 μm) containing the dorsal striatum were obtained 4–8 weeks after AAV injection using standard techniques[50]. Briefly, animals were anesthetized with isoflurane and decapitated. The brain was exposed and chilled with ice-cold artificial cerebrospinal fluid (ACSF) containing 125 mM NaCl, 2.5 mM KCl, 2 mM $CaCl_2$, 1.25 mM NaH_2PO_4, 1 mM $MgCl_2$, 25 mM $NaHCO_3$, and 15 mM D-glucose (300–305 mOsm). Brain slices were prepared with a vibrating microtome (Leica VT1200 S, Germany) and left to recover in ACSF at 34 °C for 30 min followed by room temperature (20–22 °C) incubation for at least additional 30 min before transfer to a recording chamber. The slices were recorded within 5 hours after recovery. All solutions were saturated with 95% O_2 and 5% CO_2 (Carbogen) in ACSF, which was pumped out of the recording chamber using a Masterflex HV-77122-24 pump. Hippocampal CA1 layer pyramidal neurons were visualized with infrared differential interference contrast (DIC) illumination and ASAP3/4b-Kv-expressing neurons were identified with epifluorescence illumination on a BX-51 microscope equipped with a 60× 1.0-NA water-immersion objective and DIC optics (Olympus) and a Lambda XL arc lamp (Sutter Instrument). Whole-cell current-clamp recording was performed with borosilicate glass microelectrodes (3–5 MΩ) filled with a K^+ based internal solution (135 mM KCH_3SO_3, 8.1 mM KCl, 10 mM HEPES, 8 mM Na_2phosphocreatine, 0.3 mM Na_2GTP, 4 mM MgATP, 0.1 mM $CaCl_2$, 1 mM EGTA, pH 7.2–7.3, 285–290 mOsm). Access resistance was compensated by applying bridge balance. To induce firing, 1-ms pulses of 2-nA current were injected to induce spiking at 10, 20, or 50 Hz, or constant currents were injected starting at 100 pA and increasing by 50–100 pA until spiking was elicited, and then continued until spikes began to attenuate due to the depolarization blockade. Recordings were obtained with a Multiclamp 700B amplifier (Molecular Devices) using the WinWCP software (University of Strathclyde, UK). Signals were filtered with a Bessel filter at 2 kHz to eliminate high frequency noise, digitized at 10 kHz (NI PCIe-6259, National Instruments).

Two-photon imaging was performed with a custom built two-photon laser-scanning microscope as described previously[51], equipped with a mode-locked tunable (690–1040 nm) Mai Tai eHP DS Ti:sapphire laser (Spectra-Physics) tuned to 940 nm. The jRGECO signal in the red channel was ultimately not included because this setup was not able to obtain jRGECO signals at 940 nm, and did not have enough power at higher wavelengths to obtain a good signal in the red channel. ASAP signals were acquired by a 1-kHz line scan across the membrane region of a cell at powers of 130–150 mW. Signals recorded along each line were integrated to produce a fluorescence trace over time, and a region of the line scan corresponding to the background beyond the cell membrane was chosen as the background value, and subtracted from the integrated membrane region. All traces were then normalized to 1.0 by either dividing by a monoexponential, or dividing by the first 0.5 s of data where no activity was present, if there was no photobleaching present and the exponential fit was not working well.

For the SNR calculation, the formula $\Delta F/F_0$ divided by the standard deviation (SD) of F_0 was used. F_0 was determined by using the value of the monoexponential or linear fit right before the spike occurred in the raw data. To calculate SD, the 50 points immediately preceding the detected spike peak in the raw data were used. F is the maximum value attained by each spike after the trace was normalized to 1 by dividing by a monoexponential fit to the trace. The data points ± 2 ms of the peak of the average fluorescence waveform were searched to find the peak of single spikes, in order to account for timing jitter in the recordings. For the current steps, spikes were included in the SNR comparisons and average waveforms if the corresponding electrophysiological waveform crossed 20 mV in height at its peak. This excluded attenuated spikes from the analysis. Once detected in the data, spikes were aligned to where the electrophysiology trace crossed the 20mV threshold.

Spike onset times for current step spikes were also determined by where the electrophysiology trace first crosses 20mV. The fluorescence traces were aligned to this threshold crossing, and the difference between the peak of the mean fluorescence trace and this threshold crossing in the electrophysiological trace taken to be the average delay time. The standard deviation was determined by finding the peak in the individual fluorescence responses within a 3ms window of time from when the average peak occurred for that respective protein, giving each trace an average time delay value +/− a standard deviation. For the ISI histograms, the time between spikes during current step application were sorted into 20 histogram bins in 10-ms increments, from ISIs of 10 to 200 ms. Anything larger than 200 ms was added to the 200-ms bin, giving a slight bump at the 200ms bin."

In vivo two-photon imaging of ASAP4e and jRGECO1a in the visual cortex.

Wild-type C57Bl/6 mice (Jackson Laboratories #000664) were used for simultaneous calcium and voltage imaging. A cranial window was implanted as described previously [52]. In brief, a 3-month-old mouse was administered 1–2% isoflurane in O_2 by inhalation for anesthesia and bunprenorphine for analgesia, then head-fixed in a stereotax. A craniotomy was made over the left V1 region, followed by injection at 300 μm below the exposed brain surface of 200 nL of a 3:1 mixture of AAV8-Syn-ASAP4e-Kv (from 6.21×10^{11} GC/mL stock) and AAV1-Syn-NES-jRGECO1a (from 1×10^{11} GC/mL stock, Addgene #100854).

A glass window was embedded and sealed in the craniotomy. A stainless-steel head-bar was firmly attached to the skull with dental acrylic. The implanted mouse was provided with the post-operative analgesic Meloxicam for 2 days and allowed to recover for 2 weeks prior to imaging.

Imaging was performed on awake head-fixed mice. A modified, commercially available two-photon microscope was used[28]. A titanium-sapphire laser (Chameleon Ultra II, Coherent Inc.) was used as the two-photon excitation source, and a wavelength of 1000 nm was chosen to excite both ASAP4e-Kv and jRGECO1a fluorescent proteins. Post-objective powers of 18–31 mW were used for imaging of depths 140–185 μm below brain surface. Fields of view from 32×32 μm to 240×240 μm were imaged at a pixel size of 0.25×0.25 μm/pixel, resulting in frame rates varying from 15-99Hz. Images from two fluorescence emission channels (green: ASAP4e-Kv, red: jRGECO1a) were collected simultaneously. Image time stacks were first registered with rigid motion correction (NoRMCorre, MATLAB), then single neuron time traces were extracted by averaging the signal within hand-drawn ROIs using Fiji (ImageJ).

In vivo one-photon imaging of hippocampus during running.

Adult (11–23 weeks old) SST-IRES-Cre mice (2 male, 5 female) were injected with 500 nL of either AAV8-EF1α-DiO-ASAP3-Kv at a titer of 2.4×10^{12} GC/mL (2 mice), AAV8-eEFα-DiO-ASAP4b-Kv at a titer of 2.4×10^{12} GC/mL (2 mice), or AAV8-EF1α-DiO-ASAP4e-Kv at a titer of 3.45×10^{11} GC/mL (4 mice), in the right dorsal CA1 area at 60 nL/min. 455-nm light was used as it has been shown to increase photostability over 470 nm in ASAP family GEVIs [53]. We kept maximum LED power at 5 mW total and 250 mW/mm² or less, as we found, and it has been previously shown, that sustained power levels above this resulted in tissue damage[54]. Data was acquired at 1000 fps while the mice ran on a wheel, in 11-s behavioral intervals. In between each 11-s recording bout was an 8.1-s pause. All surgical procedures, injection site, postoperative and training protocols are as previously described[55].

Animals were imaged using a custom-built, high-speed single-photon epi-fluorescent microscope. Photoexcitation was provided via a fiber-coupled LED (Thorlabs, M455F3) with a center wavelength of 455nm [53]. Excitation light is collimated after a 2-m long, 400-μm core multi-mode fiber optic patch cord (Thorlabs, M28L02) and expanded using a Keplerian telescope. The expanded beam is passed through a spectral excitation filter (Thorlabs, MF455-45), and reflected off of a long-pass dichroic mirror (Thorlabs, MD480) before teaching a 16× 0.8-NA water-immersion objective (Nikon, CFI75 LWD 16×W). The expander is used to generate a localized excitatory spot ~165 μm in diameter, at the focal plane. Emitted fluorescence is collected and transmitted through the dichroic mirror and an emission filter (Thorlabs, MF530-43) before reaching a 100-mm tube lens (Thorlabs, AC300-100-A) to form an image on a fast scientific CMOS camera (Hamamatsu Photonics, ORCA-Lightning C12120-20P) capable of kilohertz framerates. HCImage (Hamamatsu) was used for image acquisition. Excitatory power (mW) was measured on a power meter (Thorlabs PM100D, S130C sensor) before each experiment and converted to irradiance (mW/mm²) within the excitatory spot area for direct comparisons between datasets.

Time series data was extracted by first motion correcting the videos using NoRMCorre (MATLAB). ROIs were then drawn by hand in Fiji and mean fluorescence measured across time. Mean intensity from a background ROI was subtracted at each timepoint, then traces were time-binned to 500 fps and intensities normalized to the earliest stable baseline. For examples of spiking activity before and after photobleaching, 500-fps traces were exhibited without filtering or flattening. For measurements of photostability in neurons, traces were time-binned to 1 fps to reduce the contribution of shot noise to the variance between neurons. For spike statistics, traces were flattened by dividing it by a lowpass filtered version of itself using a 0.5- to 2-Hz lowpass second-order butterworth filter. This had the desired effect of capturing small changes due to movement and eliminating them, something a monoexponential fit did not do well. The data was then put through our spike detection algorithm, choosing a minimum of 10 spike templates per cell. To obtain the theta phase, we bandpass filtered the fluorescence traces between 6 and 11 Hz using a first-order Butterworth filter, giving us the theta frequency band. We then applied the Hilbert transform, giving us the instantaneous amplitude and phase of the bandpass filtered signal. We were able to detect a very consistent relationship between theta phase and spiking across all mice and all indicators, with spike likelihood peaking at 0 radians (Fig. 4E). Note that the ASAP3-Kv plot was flipped; as ASAP3 is a negatively tuned indicator, it would produce theta rhythms with peaks at pi radians off from the positive indicators if its response were not flipped. To generate images of ASAP-expressing neurons for display, images were spatially upsampled by 4× in each dimension and then aligned using the Fiji Template Matching plugin, and a maximum intensity projection of the new time series was made. This mimicked a long time exposure while minimizing blurring caused by motion.

In vivo one-photon voltage imaging from mouse motor cortex during running.

Stereotaxic viral injection and cranial window surgery were conducted in 6-week-old wild-type C57BL/6J male mouse (Jackson Laboratories #000664) as previously described[56]. Briefly, two viruses were mixed in saline (AAV-EF1α-Flex-ASAP4e-Kv (2.9×10^{12} GC/mL), and AAV-hSyn-Cre (2.0×10^{13} GC/mL)) prior to injection, but the latter was diluted at 1/1000 in volume which resulted in ~100× less Cre-recombinase virus in titer relative to the ASAP4e-Kv virus to achieve sparse labeling. The mouse was anesthetized using 1.5–2.0% isoflurane and then 500 nL of the viral mixture was injected in the left hemisphere at 1.0 mm AP, −1.5 mm ML, and 1.5 mm DV. After four weeks of recovery, a 3×3 mm cranial window (#1 glass coverslip) was implanted over the injection site using dental cement (Parkell C&B Metabond). A titanium headplate was attached to the skull to immobilize the mouse head during subsequent imaging on the running wheel.

Four weeks after the cranial window surgery, mice were placed on a custom-made running wheel to acquire spontaneous brain activity from primary motor cortex layer 1. A BX-51 microscope (Olympus) equipped with a long-working distance (2.0 mm) 20× 1.0-NA objective (Olympus XLUMPlanFLN), a 470-nm LED (SOLIS-470C, Thorlabs), and a FITC-5050A filter set (Semrock) were used for excitation. The field aperture diaphragm was closed to the minimum size to improve signal-to-background ratio as previously described[57]. High-speed images were acquired by a Flash4.0 V2 CMOS camera (Hamamatsu C11440–22CA) controlled by HCImage Live software (Hamamatsu). Spatial binning (4×4), and

cropping (512×128 pixels) were used to achieve a framerate of 384 fps. Images were saved in DCIMG file format, then converted to TIFF files in MATLAB (Mathworks) with a manufacturer-provided DCIMG reader for subsequent image analyses. The acquired TIFF stack image was further cropped using NIH Fiji to retain only the field of illumination. We then used a custom-written motion correction algorithm based on pyStackReg to register rigid motions in the stack. Cellular and background ROIs were manually selected, then background-subtracted signals were normalized to initial values. To generate the image of ASAP4e-Kv-expressing neuron for display, the original TIFF stack file was spatially up-sampled, and then re-registered as described above, and intensities summed through the stack.

In vivo two-photon imaging of hippocampus during spatial navigation.

Prior to surgery, imaging cannula implants were prepared using similar methods to those previously published [58]. Imaging cannulas consisted of a 1.3-mm-long stainless steel cannula (3-mm outer diameter, McMaster) glued to a circular cover glass (Warner Instruments, #0 cover glass 3-mm diameter; Norland Optics #81 adhesive). Excess glass overhanging the edge of the cannula was shaved off using a diamond tip file. C57BL/6J mice (Jackson Laboratory stock #000664) were first anaesthetized by an intra-peritoneal injection of a ketamine/xylazine mixture. Before the start of the surgery, animals were also subcutaneously administered 0.08 mg Dexamethasone, 0.2 mg Carprofen, and 0.2 mg Mannitol. After one hour, animals were maintained under anesthesia via inhalation of a mixture of oxygen and 0.5–1% isoflurane. Then, 500 nL of a virus mixture (AAV8-syn-ASAP4b-Kv-WPRE at $1.17×10^{12}$ GC/mL final; AAV1-syn-NES-jRGECO1b-WPRE-SV40 at $1.3×10^{13}$ GC/mL final, Addgene #100857) was injected into the left hippocampus (500 nL injected at −1.8 mm AP, −1.1 mm ML, 1.4 mm DV) using a 36-gauge Hamilton syringe (World Precisions Instruments). The needle was left in place for 15 min to allow for virus diffusion. The needle was then retracted and the imaging cannula implant was performed.

A 3-mm-diameter craniotomy was performed over the left posterior cortex (centered at −2 mm AP, −1.8 mm ML). The dura was then gently removed and the overlying cortex was aspirated using a blunt aspiration needle under constant irrigation with sterile artificial cerebrospinal fluid (ACSF). Excessive bleeding was controlled using gel foam that had been torn into small pieces and soaked in sterile ACSF. Aspiration ceased when the fibers of the external capsule were clearly visible. Once bleeding had stopped, the imaging cannula was lowered into the craniotomy until the cover glass made light contact with the fibers of the external capsule. In order to make maximal contact with the hippocampus while minimizing distortion of the structure, the cannula was placed at approximately a 10° roll angle relative to the animal's skull. The cannula was then held in place with cyanoacrylate adhesive. A thin layer of adhesive was also applied to the exposed skull. A number-11 scalpel was used to score the surface of the skull prior to the craniotomy so that the adhesive had a rougher surface on which to bind. A headplate with a left-offset 7-mm diameter beveled window was placed over the secured imaging cannula at a matching 10-degree angle, and cemented in place with Met-a-bond dental acrylic that had been dyed black using India ink to prevent VR light from coming into the objective.

At the end of the procedure, animals were administered 1 mL of saline and 0.2 mg of Baytril and placed on a warming blanket to recover. Animals were typically active within 20 min and were allowed to recover for several hours before being placed back in their home cage. Mice were monitored for the next several days and given additional Carprofen and Baytril if they showed signs of discomfort or infection. Mice were allowed to recover for at least 10 days before beginning water restriction and VR training.

All virtual reality environments were designed and implemented using the Unity game engine (https://unity.com/). Virtual environments were displayed on three 24-in LCD monitors that surrounded the mouse and were placed at 90° angles relative to each other. A dedicated PC was used to control the virtual environments and behavioral data was synchronized with calcium imaging acquisition using transistor-transistor logic (TTL) pulses sent to the scanning computer on every VR frame. Mice ran on a fixed-axis foam cylinder, and running activity was monitored using a high precision rotary encoder (Yumo). Separate Arduino Unos were used to monitor the rotary encoder and control the reward delivery system.

In order to incentivize mice to run, the animals' water intake was restricted. Water restriction was not implemented until 10–14 days after the imaging cannula implant procedure. Animals were given 0.8–1.0 mL of 5% sugar water each day until they reached ~85% of their baseline weight and given enough water to maintain this weight.

Mice were handled for 3 days during initial water restriction and watered through a syringe by hand to acclimate them to the experimenter. On the fourth day, we began acclimating animals to head fixation (day 4: ~30 min, day 5: ~1 h). After mice showed signs of being comfortable on the treadmill (walking forward and pausing to groom), we began to teach them to receive water from a "lickport". The lickport consisted of a feeding tube (Kent Scientific) connected to a gravity fed water line with an in-line solenoid valve (Cole Palmer). The solenoid valve was controlled using a transistor circuit and an Arduino Uno. A wire was soldered to the feeding tube and capacitance of the feeding tube was sensed using an RC circuit and the Arduino capacitive sensing library. The metal headplate holder was grounded to the same capacitive-sensing circuit to improve signal-to-noise, and the capacitive sensor was calibrated to detect single licks. The water delivery system was calibrated to deliver ~4 µL of liquid per drop.

After mice were comfortable on the ball, we trained them to progressively run further distances on a VR training track in order to receive sugar water rewards. The training track was 450 cm long with black and white checkered walls. A pair of movable towers indicated the next reward location. At the beginning of training, this set of towers were placed 30 cm from the start of the track. If mouse licked within 25 cm of the towers, it would receive a liquid reward. If the animal passed by the towers without licking, it would receive an automatic reward. After the reward was dispensed the towers would move forward. If the mouse covered the distance from the start of the track (or the previous reward) to the current reward in under 20 seconds, the inter-reward distance would increase by 10 cm. If it took the animal longer than 30 seconds to cover the distance from the previous reward, the inter-reward distance would decrease by 10 cm. The minimum reward distance was set to

30 cm and the maximal reward distance was 450 cm. Once animals consistently ran 450 cm to get a reward within 20 s, the automatic reward was removed and mice had to lick within 25 cm of the reward towers in order to receive the reward. After the animals consistently requested rewards with licking, we began training on tracks used for imaging.

Two visually distinct VR tracks were used for imaging. Each track was 200 cm in length with a 50-cm hidden reward zone. In the first VR track, the 50-cm reward zone was the last 50 cm of the track, and in the second VR track, the 50-cm reward zone began 75 cm down the VR track so that it was in the middle of the track. Mice had to lick within the reward zone in order to receive liquid rewards. At the end of each trial, the animal was teleported to a dark hallway for a randomly determined timeout period of 5–10 s, chosen with equal probability for each possible timout length. During this timeout period, the laser power was reduced to 0 mW in order to reduce excessive photobleaching. After the timeout period finished, the laser power was increased and the mouse self initiated the beginning of the next trial by running forward. Data from both VR tracks was included in all analyses.

To image the calcium and voltage activity of populations of neurons in CA1, we used a resonant galvonometer-scanning two-photon microscope (Neurolabware). All data was collected using a 25× 1.0-NA objective (Leica HC IRAPO). Neurolabware microscope firmware was modified to allow continuous bidirectional scanning at 989 Hz without digitizer buffer overload (16×796 pixels, 0.02×0.64-mm field of view). 940-nm light (Coherent Discovery laser) was used for excitation of both jRGECO1b and ASAP4b-Kv in all cases. Laser power was controlled using a pockels cell (Conoptics). Laser power was set on each session to obtain satisfactory SNR with the least amount of power possible. For ASAP4b-Kv imaging, the power ranged from 366 to 645 mW/mm^2. Light was collected using photomultiplier tubes (Hamamatsu H10770B-40 and H11706-40 MOD for green and red channels respectively).

Data was motion-corrected using the motion correction pipeline from the Suite2P software package[36]. Putative CA1 cell membrane segments were circled by hand using the motion corrected average ASAP4b-Kv image from each session in ImageJ (imagej.nih.gov). Given the dense labeling of cells as well as the dense cell packing of the CA1 pyramidal cell layer, some of the membrane segments likely contain signals mixed from several cells. Based on the numerical aperture of the objective and our approximate axial resolution, we estimate that each ROI contains signal from (~1–3) cells. Pixel-averaged timeseries were extracted from both the red and green channels for each ROI.

For each ROI, we calculated F/F independently for the green and red channels. Since laser power was set to 0 mW between each trial, signal baseline was calculated independently on each trial as well. Due to the small FOV and the fact that animals were running at high speeds (~40 cm/s) some frames were not able to be accurately motion corrected. We attempted to remove the effect of these high-motion frames from our analyses by using Suite2P's motion estimates to calculate which frames were corrupted by motion. Any frame within 20 frames of one of these high motion frames was replaced with a "NaN" value. Motion estimates from Suite2P rigid motion correction were then used as nuisance regressors for the remaining timepoints, with the following design matrix:

$X = [x(t), y(t), x^2(t), y^2(t), x(t)x(t)]$. The residual timeseries from this regression were used for the remaining analyses. For baseline calculation, NaNs were linearly interpolated from the surrounding frames. These motion-imputed timeseries were then low pass filtered to calculate a baseline timeseries (green channel: 0.5 Hz 8th order Butterworth low pass filter, red channel: 0.25 Hz 8th order Butterworth low pass filter). Residual ROI timeseries (NaNs included) were divided by this baseline to get F/F. For place cell identification and visualization, F/F was convolved with a 5-frame Gaussian.

Place cells were identified using a previously published spatial information (SI) metric[36],

$$SI = \sum_j P_j \lambda_j \frac{\lambda_j}{\lambda},$$

where λ_j is the average activity rate of a cell in position bin j, λ is the position-averaged activity rate of the cell, and p_j is the fractional occupancy of bin j. The track was divided into 10 cm bins, giving a total of 20 bins. To determine the significance of the SI value for a given cell, we created a null distribution for each cell independently using a shuffling procedure. On each shuffling iteration, we circularly permuted the cell's time series relative to the position trace within each trial and recalculated the SI for the shuffled data. Shuffling was performed 100 times for each cell, and only cells that exceeded all 95% of permutations were determined to be significant "place cells".

To further ensure the reliability of the place cells, we implemented split-halves cross-validation. Taking only the odd-numbered trials, we computed the average firing rate map to identify the position of peak activity. Each cell's activity was "z-scored" based on the mean and standard deviation across spatial bins on odd-numbered trials. Cells were sorted by this position and then the average activity on even-numbered trials was plotted. This gives a visual impression of the reliability of the place cells. For visualization, single trial activity rate maps were smoothed with a 20-cm (2 spatial bins) Gaussian kernel.

Gaussian log-likelihood-based signal detection.

Our spike detection framework builds on a previously published log likelihood ratio based framework by Wilt et al[30]. To implement the equations in that study on real-world empirical data, we changed the assumed dominant noise structure from Poisson-distributed shot noise to Gaussian distributions. We found noise in our measurements was primarily Gaussian in nature, likely because electronic sources dominated over photon shot noise.

Spike templates were chosen for each imaging session, and were chosen to be the largest spiking events from the beginning of the session, with a minimum of 10 chosen each time. Naturally, as photobleaching occurred across trials and spikes become noisier, fewer were detected since the template spikes were taken from the initial imaging period and were thus much larger. While taking only the largest events to use as the template results in very conservative detection, with smaller, noisier events remaining undetected, we wanted to be confident in the events we did detect, and felt that this was a safer approach. The red line represents the significance threshold, which was chosen such that after breaking the data vector into pieces with lengths equal to the length of the spike template, there was a 1/(20

× number of pieces) chance of getting a false positive in any given piece of data. This was done to correct for multiple comparisons.

Once the event templates were chosen, the equations and procedures described below allow the data to be converted into a probability vector. The probability vector quantifies the probability that the data came from the distribution defined by the templates. N is the length of the templates in samples (time bins), and the data is taken in N samples at a time and compared to it. The background also has a template of length N, but since our data was normalized to 1, we set the background to a vector of ones of length N. See the section below on Background Noise Estimation for how we estimated the standard deviation of the background template. Our new gaussian equations for calculating the log likelihood probability that the observed data came from the distribution defined by the template events are as follows:

For time bins where the k'th mean template value is less than the k'th value of the background, where k only counts the time bins where this condition is true: U is the total number of time bins where the mean of the templates are less than the mean of the background. f_k is the k'th sample of the new data being analyzed.

$$Chance\ Noise\ Under_k = \prod_{k=1}^{U} \int_{-\infty}^{f_k} N(\mu_{Bk}, \sigma_{Bk})$$

μ_{Bk} is the mean of the mean of the background template at the k'th data point. For our purposes this was the number 1 for all k since we normalized the data, but it does not have to be. σ_{Bk} is the standard deviation of the background at the k'th point. See the "Background noise estimation" for how this was estimated.

$$Chance\ Signal\ Under_k = \prod_{k=1}^{U} \int_{f_k}^{\infty} N(\mu_{Sk}, \sigma_{Sk})$$

μ_{Sk} is the mean of the templates the user selected at the k'th point. Note that this allows for the shape of the event to be taken into account when calculating probabilities. σ_{Sk} is the standard deviation of the k'th time bin for the templates chosen. This means that each time bin of the event template has its own mean and standard deviation, creating N gaussian distributions, which are needed to take the gaussian integrals at each time bin. N is the length of the templates in time bins.

Below, for time bins when the j'th mean template value is greater than the j'th value of the background, where j only counts the time bins where this condition is true: O is the total number of time bins where the mean of the templates are greater than the mean of the background. f_j is the j'th sample of the new data being analyzed.

$$Chance\ Noise\ Over_j = \prod_{j=1}^{O} \int_{f_j}^{\infty} N(\mu_{Bj}, \sigma_{Bj})$$

$$Chance\ Signal\ Over_j = \prod_{j=1}^{O} \int_{-\infty}^{f_j} N(\mu_{Sj}, \sigma_{Sj})$$

This is the same as above, only for time bins where $\mu_{Bj} < \mu_{Sj}$, so the limits of integration change.

These probabilities are multiplied together, the log of the ratio of them obtained, and ultimately a single number for the i'th sample of the data vector is returned, where i runs from 1 to the length of the data vector.

$$L_i = ln\left(\frac{\prod_{k=1}^{U} Chance\ Signal\ Under_k * \prod_{j=1}^{O} Chance\ Signal\ Over_j}{\prod_{k=1}^{U} Chance\ Noise\ Under_k * \prod_{j=1}^{O} Chance\ Noise\ Over_j}\right)$$

Note that since N is the length of the template in samples, $N = U + O$.

This is repeated, each time shifting over by a single time bin in the data, until the entire data vector has been analyzed and converted into a probability vector. The very end of the data vector is chopped as we did not find an objective way to pad the end of data vector such that it would not impact the probabilities calculated for when the template distribution reaches the end. Fortunately, our templates were typically very short in length, so this resulted in a very negligible loss of data at the very end of each data set (a few tens of milliseconds). While taking the log of the ratio here is not strictly necessary for the purposes of signal detection, it helped to keep the ratio from becoming too positive or too negative to visualize effectively when making plots.

We next find all of the events that cross the probability threshold we set. Every segment above threshold is considered a single template matching event, for as long as it stays above threshold in the log likelihood probability vector. Since it does this, it is important to set the filter parameters such that you pull out the events you care about. For example, if the user wanted to detect single spikes riding on top of depolarizing calcium waves, as well as the depolarizing waves themselves, you would first set a very low frequency lowpass filter as the baseline calculation, and choose the entire duration of the burst as a template. Once you have the detected bursts pulled out, you would then set the passband of the lowpass filtered calculation of the baseline higher than what was used previously to pull out the entire burst, in order to flatten out the calcium portion of the event, while maintaining the faster spikes for detection. This enables the user to sequentially detect bursts, followed by spikes within bursts.

For onset timing, the time point where the log likelihood ratio first crosses the threshold is considered the start of the event. For the event detection performed on the one-photon in vivo imaging dataset of somatostatin-positive (SST+) interneurons, we first highpass filtered both the spike templates and raw data with a 20-Hz second-order Butterworth filter.

Background noise estimation.

The standard deviation (SD) of the background template in this case is assumed to be constant across the background template. It is recalculated for each new batch of data that is fed into the program, and involves 3 successive attempts, if the previous attempt fails.

Attempt 1: The program fits a gaussian mixed model (GMM) to the entire data vector, with the assumption that there are two gaussians present. One is the signal, one is the noise. This tends to work well for traces where lots of activity is present, giving the histogram of the data vector a tail to one side; otherwise it tends to only find a single gaussian. The standard deviation of the noise is set to be the std. of the gaussian on the left if the indicator is upward going, or the gaussian on the right if it is downward going, which the program detects from the peak of the average templates. This prevents overestimating the noise, which would result in more false negatives than desired (but fewer false positives as well).

Attempt 2**:** If the SD of the GMM fit is greater than the SD of the whole data vector, then the fit is considered invalid. The program then reverts to an "asymmetric distribution technique": If the data contains signals, the distribution of the data will be skewed to one side. To the right if the indicator is upward going, and to the left if it is downward going. The side of the distribution away from the direction the indicator moves in must be pure noise, with no contamination from the signal we are looking for. That half of the distribution is then flipped about the mean to replace the half that is a mix of noise and signals, giving a good estimation of how the distribution of the data would look if there were no signals present in it. The SD of this "flipped" distribution is then taken to be the standard deviation of the noise.

Attempt 3*:* Occasionally, attempt 2 also fails, possibly due to movement or lots of hyperpolarizing activity, and the standard deviation of the flipped distribution is greater than the standard deviation of the data itself, which again does not make sense. This happens very rarely, but in this case the standard deviation of the background is simply assigned the value of the standard deviation of the entire data vector. This will have the effect of giving too many false negatives, but it has the advantage of giving fewer false positives as well, so represents a conservative estimate of spike probability.

Note that how the background noise is chosen affects the numbers in the log-likelihood vector. Less background noise will result in larger log likelihood values, and vice versa. This is because that as the noise distribution gets narrower via a smaller SD, the probability that the same data point came from the noise distribution shrinks. If there are more than 9 templates, the SD of the templates themselves are taken, as described previously, to be the SD of the templates at each time bin in the template vector. If there are less than 10 templates, the SD of the templates is assumed to be the same as the noise, and only the mean

changes (the mean template trace is still taken, but each time bin just has the same SD which is the same as the noise).

Extended Data
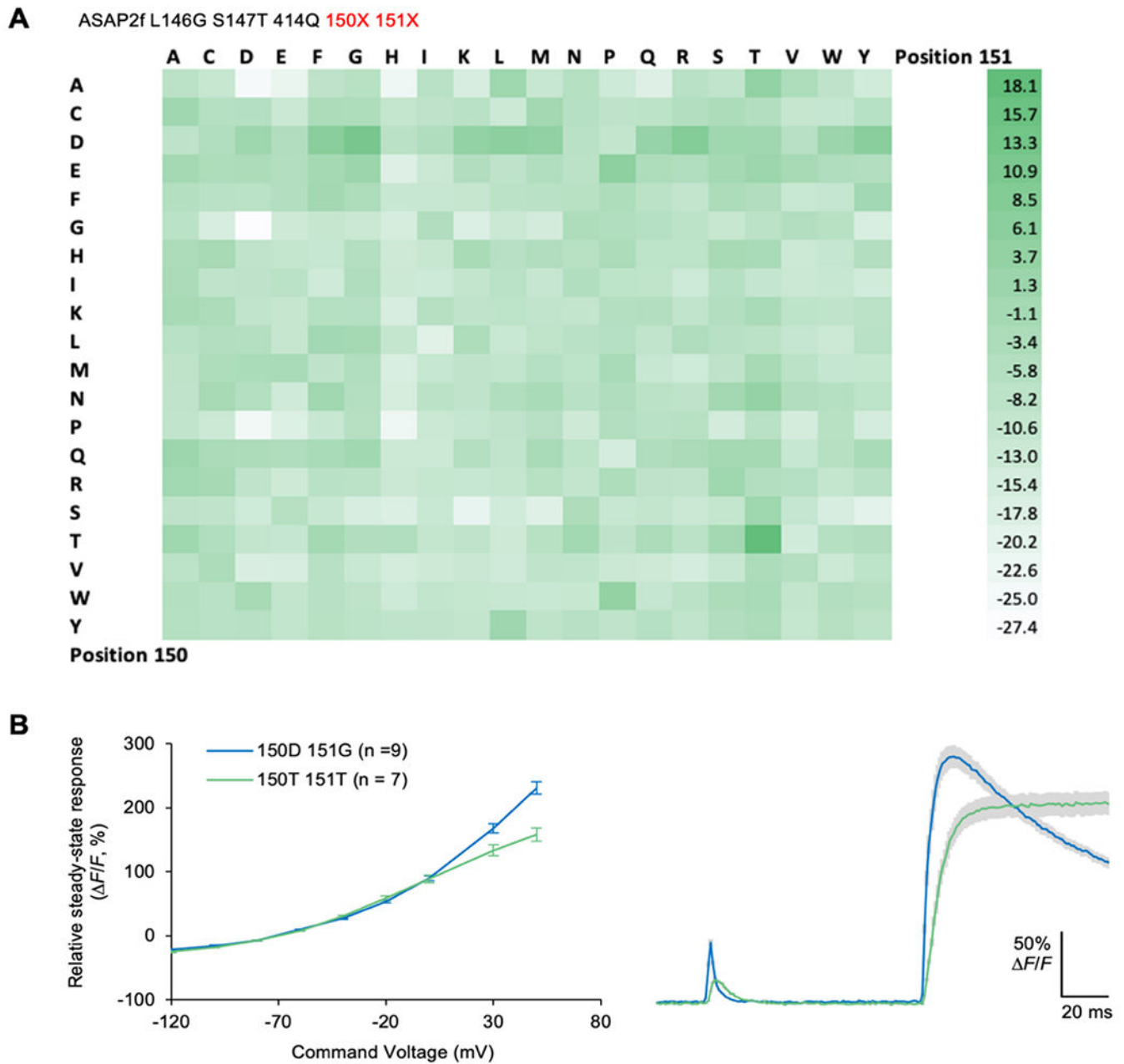
Extended Data Figure 1. Reversing the fluorescence response.
(**A**) Starting with ASAP2f L146G S147T 414Q, a predecessor to ASAP3, full-length transcription units encoding all 400 combinations of amino acids at positions 150 and 151 were generated by multiwell overlap PCR, each product directly transfected into HEK293-Kir2.1 cells in multiwell plates, and the cells screened by electroporation. Peak responses

following electroporation are shown. Note some responses to electroporation were negative (dimming) and others were positive (brightening). Mutant 150D 151G and mutant 150T 151T showed the largest positive responses. **(B)** Left, mutant 150D 151G and mutant 150T 151T were cloned into mammalian expression plasmids, expressed in HEK293A cells, and fluorescence to command voltages was measured. Responses are normalized to −70 mV. Mutant 150D 151G outperformed mutant 150T 151T in terms of responsivity. Right, mutant 150D 151G also outperforms mutant 150T 151T in activation kinetics in response to a 2-ms and 1-s steps from −70 mV to +30 mV. Mutant 150D 151G was designated ASAP4.0.
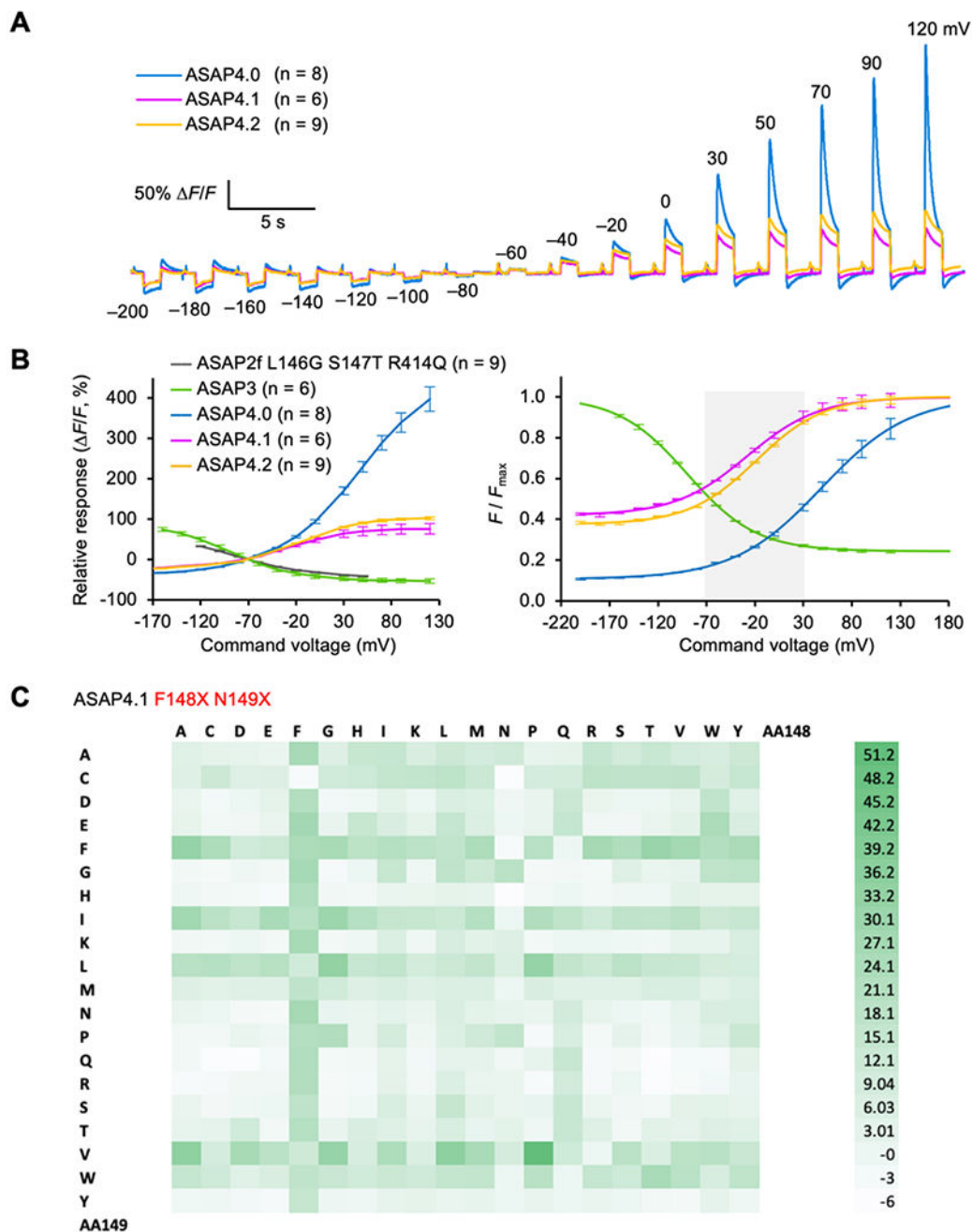
Extended Data Figure 2. ASAP4.0 to ASAP4.2.

(**A**) Steady-state responses from command voltage patch clamping in HEK 293A cells for ASAP4.0 to ASAP4.2. Responses are normalized to −70 mV. The test pulses before each step are 2-ms square steps from −70 to +30mV (**B) Left**, F/F_0 over voltage steps for the parent construct ASAP2f L146G S147T R414Q, as well as ASAP3 and the first three ASAP4 variants. Error bars are SEM. Right, brightness vs. voltage plotted as a fraction of the maximum brightness for each indicator. Data are displayed as mean ± SEM. The gray

box highlights the physiological range from −70 to +30mV. (**C**) Screening all combinations of F148X N149X in ASAP4.1 (ASAP4.0 T206H) yielded F148P N149V, creating ASAP4.2.
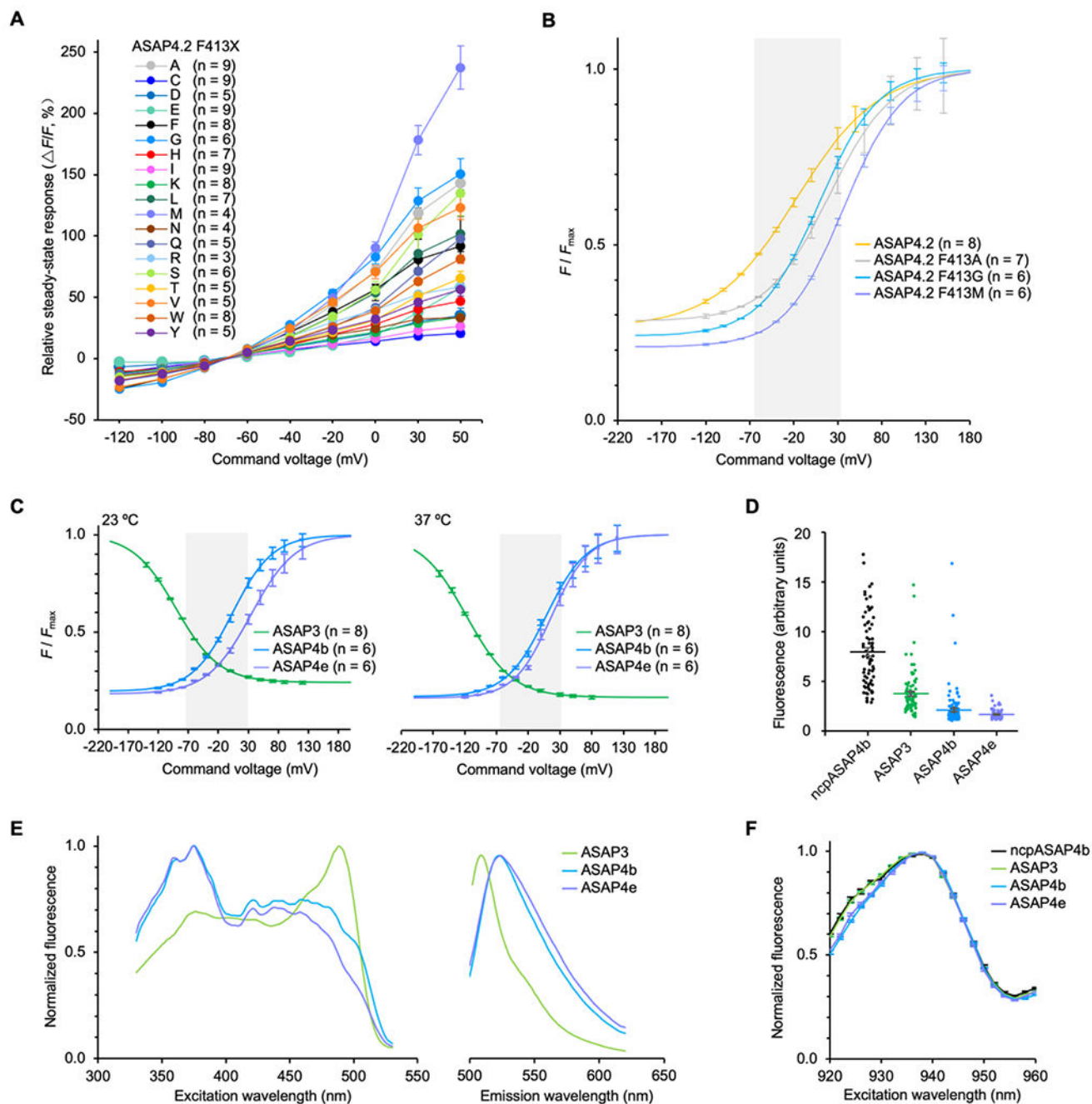
Extended Data Figure 3. Improvements to ASAP4.2.
(**A**) Mean fluorescent responses of ASAP4.2 F413X variants to a series of voltage steps from −120 to +50 mV, from a holding potential of −70 mV in voltage-clamped HEK293A cells. Error bars are standard error of the mean (SEM). Only proline was excluded due to expression issues. (**B**) F/F_{max} a 23 °C for ASAP4.2 and the three best derivatives. Error

bars represent SEM centered on measured mean values; curved lines represent Boltzmann distributions fit to the measured mean values. **(C)** F/F_{max} at 23 and 37 °C for ASAP3, ASAP4b, and ASAP4e. **(D)** F/F_{max} in HEK cells under 2-photon illumination at 940 nm for ASAP3, ASAP4b, and ASAP4e imaged at 23 °C. n = 73 for ncpASAP4b, 81 for ASAP3, 126 for ASAP4b, and 76 for ASAP4e. Bars represent mean ± SEM. All GEVIs were significantly different from each other (p < 0.0001), except for ASAP4b vs. ASAP4e (p = 0.8108) by Dunnett's multiple comparison test. **(E)** One-photon excitation and emission spectra measured for ASAP3, ASAP4b, and ASAP4e in HEK293-Kir2.1 cells at 23 °C. **(F)** Two-photon excitation spectra measured with 2-nm spectral intervals from HEK293-Kir2.1 cells. Peaks were at 938 nm. n = 52 for ncpASAP4b, 57 for ASAP3, 57 for ASAP4b, and 44 for ASAP4e.
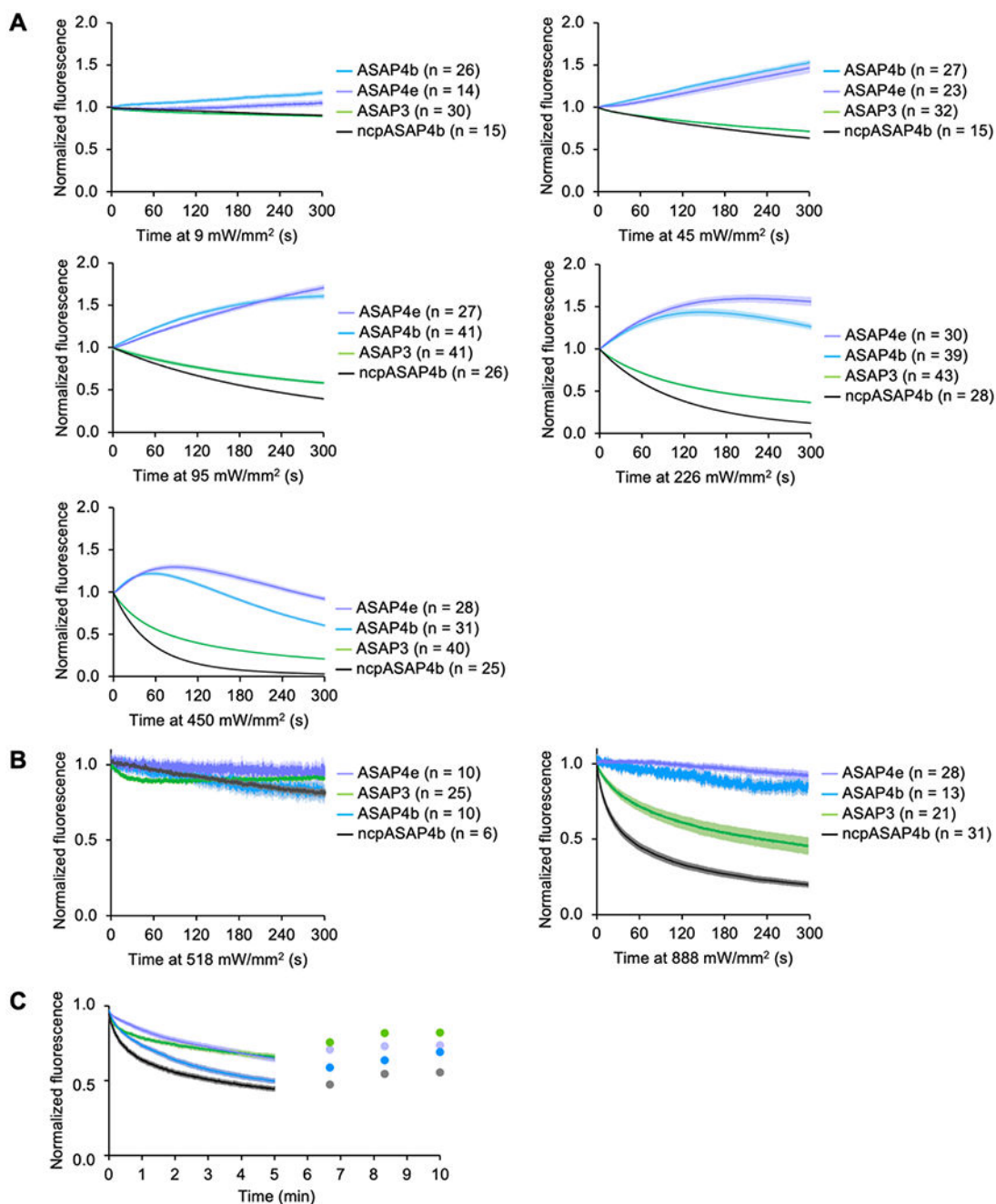
Extended Data Figure 4. Photobleaching of ASAP indicators under one-photon and two-photon excitation.
(A) One-photon photobleaching curves over 5 min of continuous illumination in cultured HEK293-Kir2.1 cells, using blue light with a peak wavelength at 453 nm, tested with varying intensities. ASAP4 variants exhibited different degrees of photoactivation depending on illumination intensity, whereas ASAP3 and ncpASAP4b did not photoactivate at any intensiry. Shaded areas represent SEM. **(B)** Resonant-scanning two-photon photobleaching in HEK293-Kir2.1 cells at 518 and 888 mW/mm^2). Shaded areas represent SEM. **(C)**

Galvanometric-scanning two-photon photobleaching in HEK293-Kir2.1 cells at 960 mW/mm^2. After 5 min, cells were incubated the dark and imaged at single time points 2.7, 3.3, and 5.0 min later. Shaded areas represent SEM.
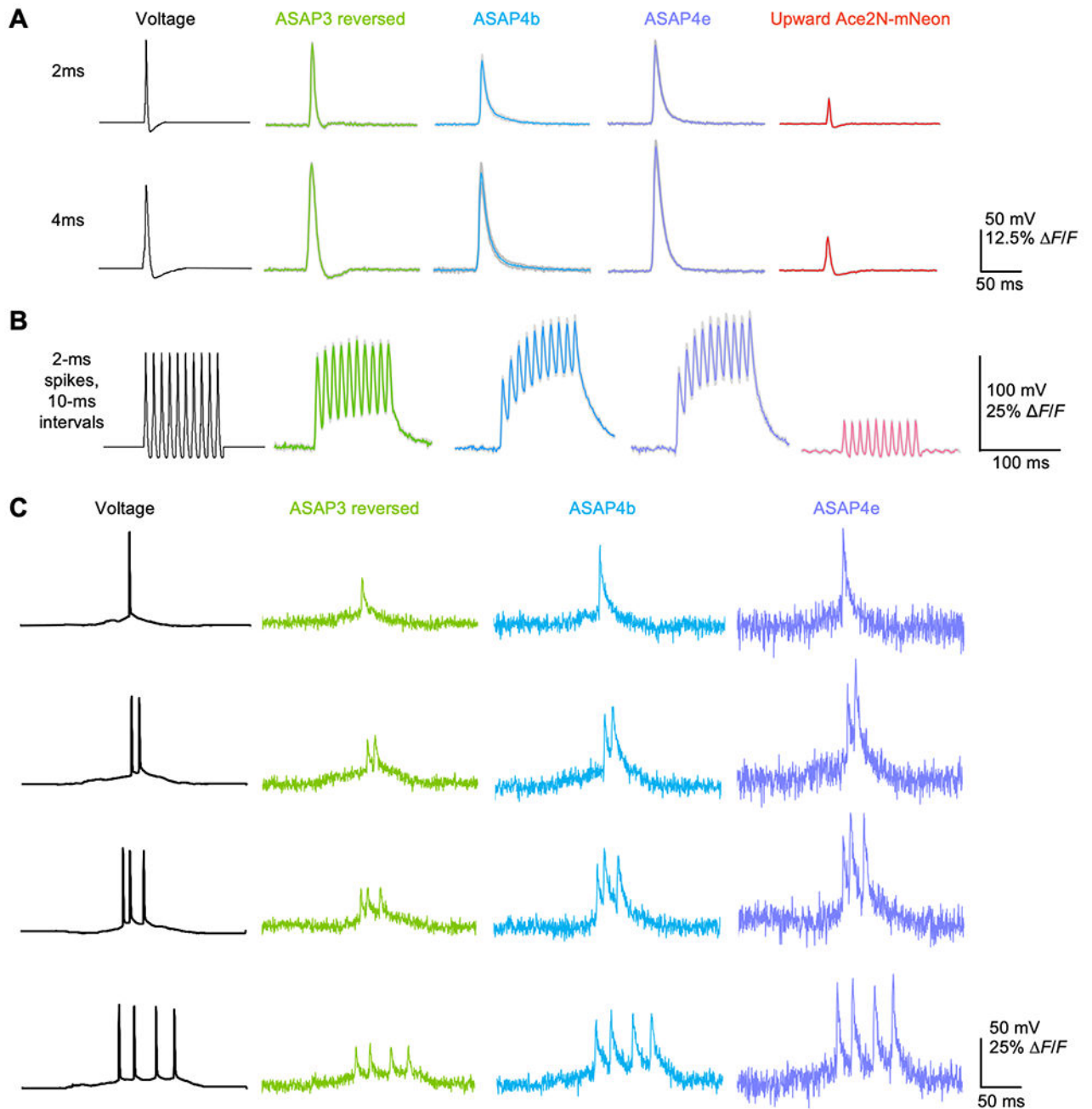
Extended Data Figure 5. Responses of ASAP family GEVIs to AP waveforms in HEK293A cells.
(A) Responses of indicators in HEK293a cells to an AP waveform (far left) under voltage clamp that has been modified to have either a 2ms FWHM (top), or a 4ms FWHM (bottom), and ranges from −70mV to +30mV. Each cell had the waveform applied 5 times, with n =

6 cells for ASAP3, n = 7 cells for ASAP4b, n = 5 for ASAP4e, and n = 7 cells for Upward Ace2mNeon. Shading is SEM. **(B)** Response to commanded spike trains in HEK293A cells at room temp. V_m was −70 mV at the start of the displayed segment and peak AP amplitude was 100 mV. Responses were collected from 6 (ASAP4.2), 7 (ASAP4b), 5(ASAP4e), 6 (ASAP3) and 7 (Upward Ace2mNeon) HEK293A cells, each supplying a single unfiltered and unsmoothed 1000-Hz trace. Colored lines represent averages, gray shading is SEM. **(C)** Responses of indicators in HEK293A cells an AP burst waveforms of 1–4 spikes with spike widths of 1.0 ms at FWHM. These waveforms were previously recorded from CA1 mouse hippocampal pyramidal neurons *in vivo*. V_m was −52 mV at the start of the displayed voltage segment. Each colored line is a single unfiltered trace with no trial averaging or filtering applied.
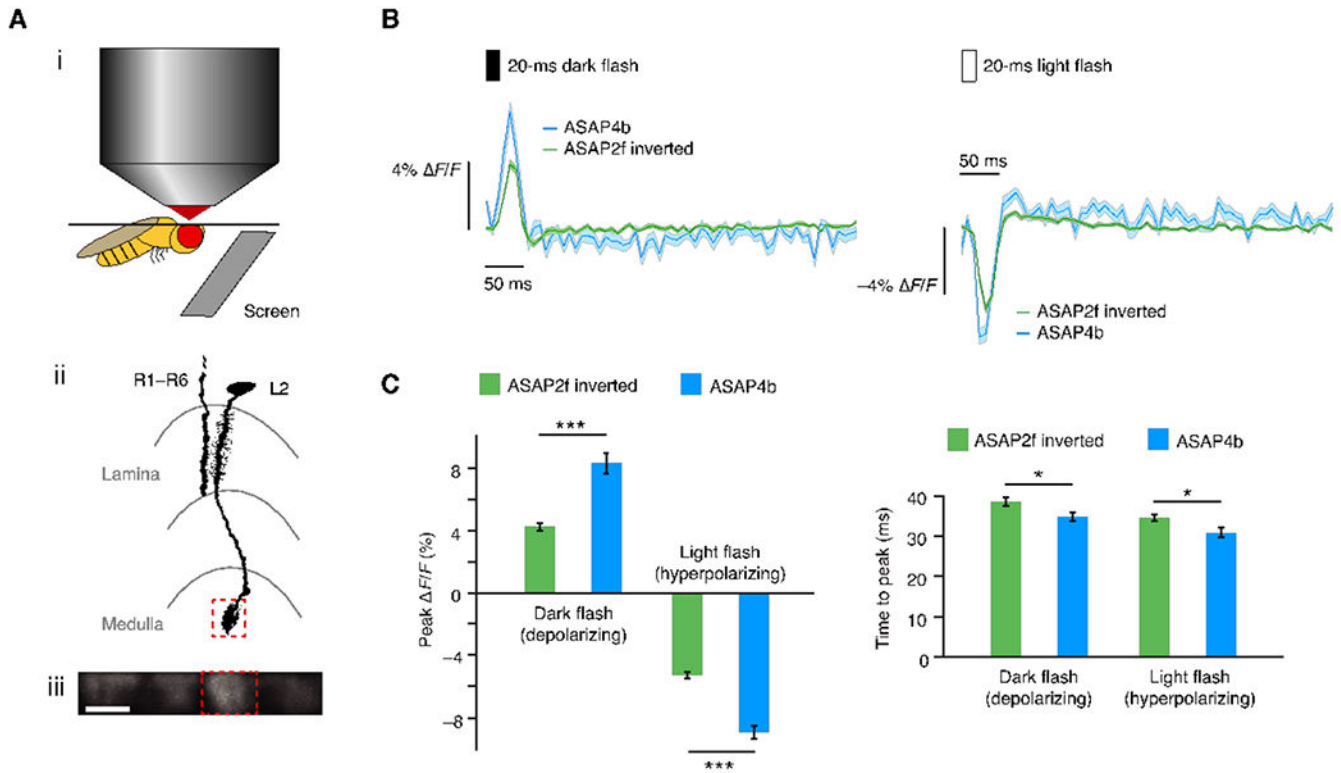
Extended Data Figure 6. Imaging ASAP4b and ASAP2f in awake flies during visual stimulation.
(A) From top to bottom: (i) Experimental setup for two-photon imaging of visually evoked responses in the *Drosophila* brain using a flickering visual stimulus on a gray background. (ii) Drawing depicting L2 non-spiking interneurons. L2 interneurons are directly postsynaptic to photoreceptors R1–R6, and depolarize to dark flashes and hyperpolarize to light flashes. Multiple L2 interneurons send axons in parallel through the lamina into the medulla, tiling visual space. (iii) Sample two-photon image of ASAP4b expression in the terminal arbors of four L2 axons. **(B)** Stimulus-evoked GEVI responses in L2 terminal arbors (n = 43 neurons from five ASAP2f flies, or 45 neurons frmo four ASAP4b flies). ASAP4b responds in the opposite direction of ASAP2f; the ASAP2f response is inverted to facilitate comparison. Flies were stimulated with a repeated sequence

of 20-ms light and dark flashes starting from a mean gray background, and then, for each arbor, stimuli-aligned responses were extracted and averaged. The solid line in the graph represents the mean waveform across all cells sampled, and the shaded area represents SEM. **(C)** Left, mean ASAP4b responses are significantly larger than ASAP2f responses to both depolarizing and hyperpolarizing stimuli. Error bars represent SEM. *** $p <$ 0.001 for depolarization (dark) and for hyperpolarization (light), using a two-sample t-test with Bonferroni correction. Right, ASAP4b produces responses with faster kinetics than ASAP2f. Plots represent mean ± SEM. * $p = 0.0406$ for depolarization (dark) and 0.0268 for hyperpolarization (light), by two-sided t-tests with Bonferroni correction.
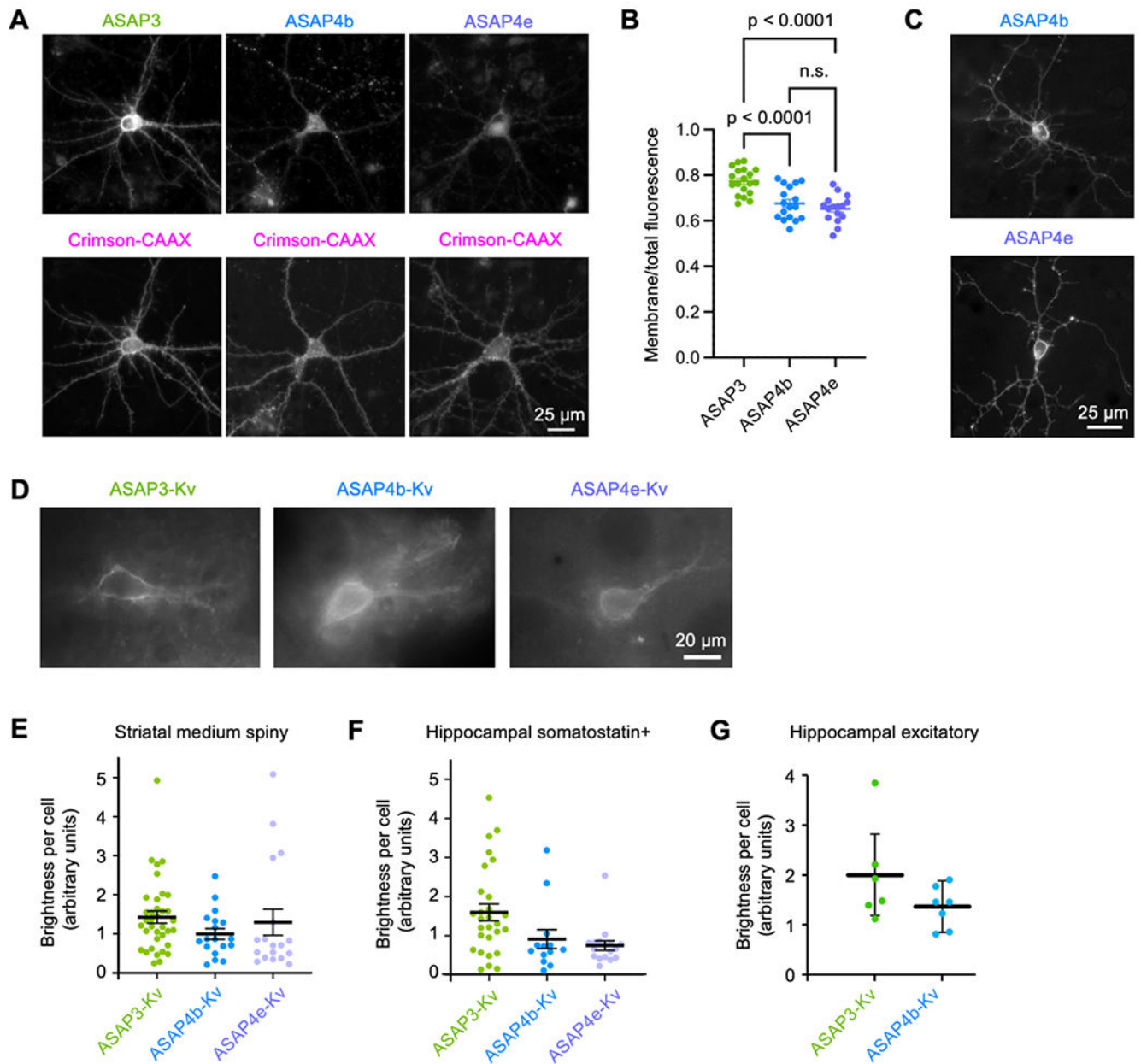
Extended Data Figure 7. Expression of pan-membrane and somatically enriched ASAP4b and ASAP4e in neurons.

(A) Example images from 15-DIV cortical neurons co-expressing ASAPs in green channel and farnesylated Crimson in red channel. **(B)** Quantification of membrane expression for none-soma targeted ASAP3 (n = 19), ASAP4b (n = 17), and ASAP4e (n = 16). The statistical significance was determined by one-way ANOVA followed by post-hoc Tukey test. **(C)** ASAP4b and ASAP4e expression in cultured hippocampal neurons from lipofection (14–15 DIV). **(D)** Examples of ASAP3-Kv, ASAP4b-Kv, and ASAP4e-Kv in acute striatal slices under one-photon illumination. Scale bar is 20 μM. **(E)** Brightness of striatal medium spiny neurons expressing somatically localized ASAPs under one-photon illumination in acute slice. n = 36 cells for ASAP3-Kv, 18 for ASAP4b-Kv, and 18 for ASAP4e-Kv, with each mouse providing 6 cells chosen randomly. Bars indicate mean ± SEM. Differences were insignificant by Kruskal Wallis test. **(F)** Brightness of SST+ hippocampal interneurons expressing somatically localized ASAPs under one-photon illumination *in vivo.* n = 28 cells for ASAP3-Kv, 13 for ASAP4b-Kv, and 17 for ASAP4e-Kv from 2–4 mice for each GEVI. Error bars are SEM. Differences were insignificant by Kruskal Wallis test. **(G)** Brightness of patch-clamped hippocampal CA1 pyramidal neurons expressing somatically localized ASAPs under 940-nm two-photon illumination. Bars indicate mean ± SEM. n = 6 cells for ASAP3-Kv and 7 for ASAP4b-Kv, with one cell per mouse. Differences in brightness were insignificant by Mann Whitney test.
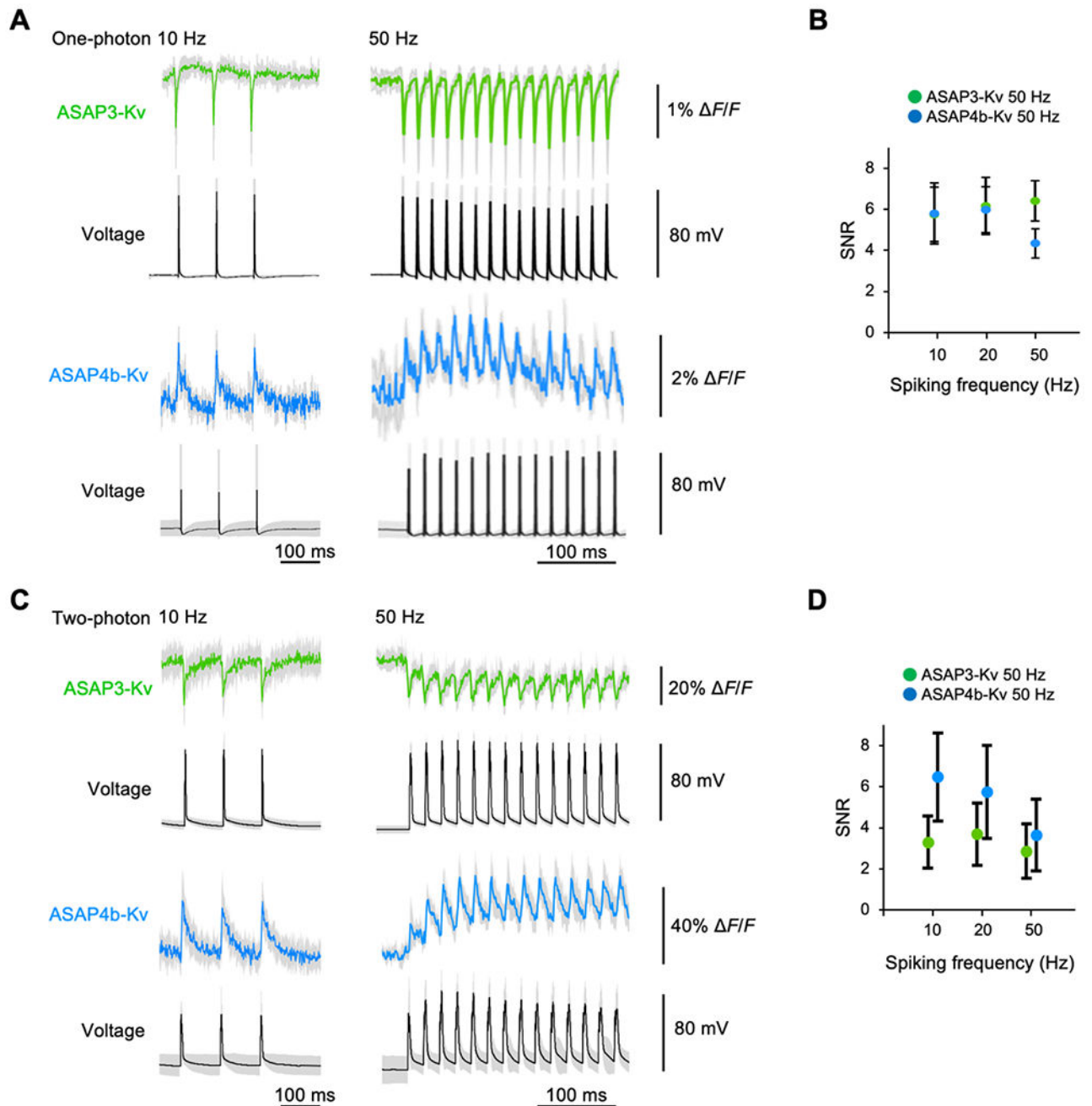
Extended Data Figure 8. Detection of 50-Hz AP trains in acute hippocampal slice.
(A) One-photon imaging of patch-clamped CA1 neurons in acute hippocampal slices expressing either ASAP3-Kv (n = 4 cells) or ASAP4b-Kv (n = 4 cells). Spike trains were evoked with current pulses, and voltage waveforms and GEVI (1000 frames per second) were recorded. Mean unfiltered responses of 12 sweeps in total are displayed with gray areas representing SEM. **(B)** Empirical SNR (F divided by SD of F_0) for single-AP one-photon responses of ASAP3-Kv and ASAP4b-Kv during spike trains. Mean ± SD is plotted. A Kruskal-Wallis test followed by Dunn's multiple comparison test was used to

compare ASAP4b-Kv to ASAP3-Kv for each spiking frequency, revealing significantly higher SNR of ASAP3-Kv at 50 Hz (multiplicity-adjusted p < 0.0001). **(C)** Two-photon imaging of pyramidal neurons in acute hippocampal slices expressing either ASAP3-Kv (n = 6 cells, 21 sweeps total) or ASAP4b-Kv (n = 5 cells, 15 sweeps total). **(D)** Empirical SNR (F divided by SD of F_0) for single-AP one-photon responses of ASAP3-Kv and ASAP4b-Kv during spike trains. Mean ± SD is plotted. A Kruskal-Wallis test followed by Dunn's multiple comparison test was used to compare ASAP4b-Kv to ASAP3-Kv for each spiking frequency, revealing significantly higher SNR for ASAP4b-Kv at all frequencies (p < 0.0001, from 475 spikes for ASAP3-Kv and 375 spikes for ASAP4b-Kv).
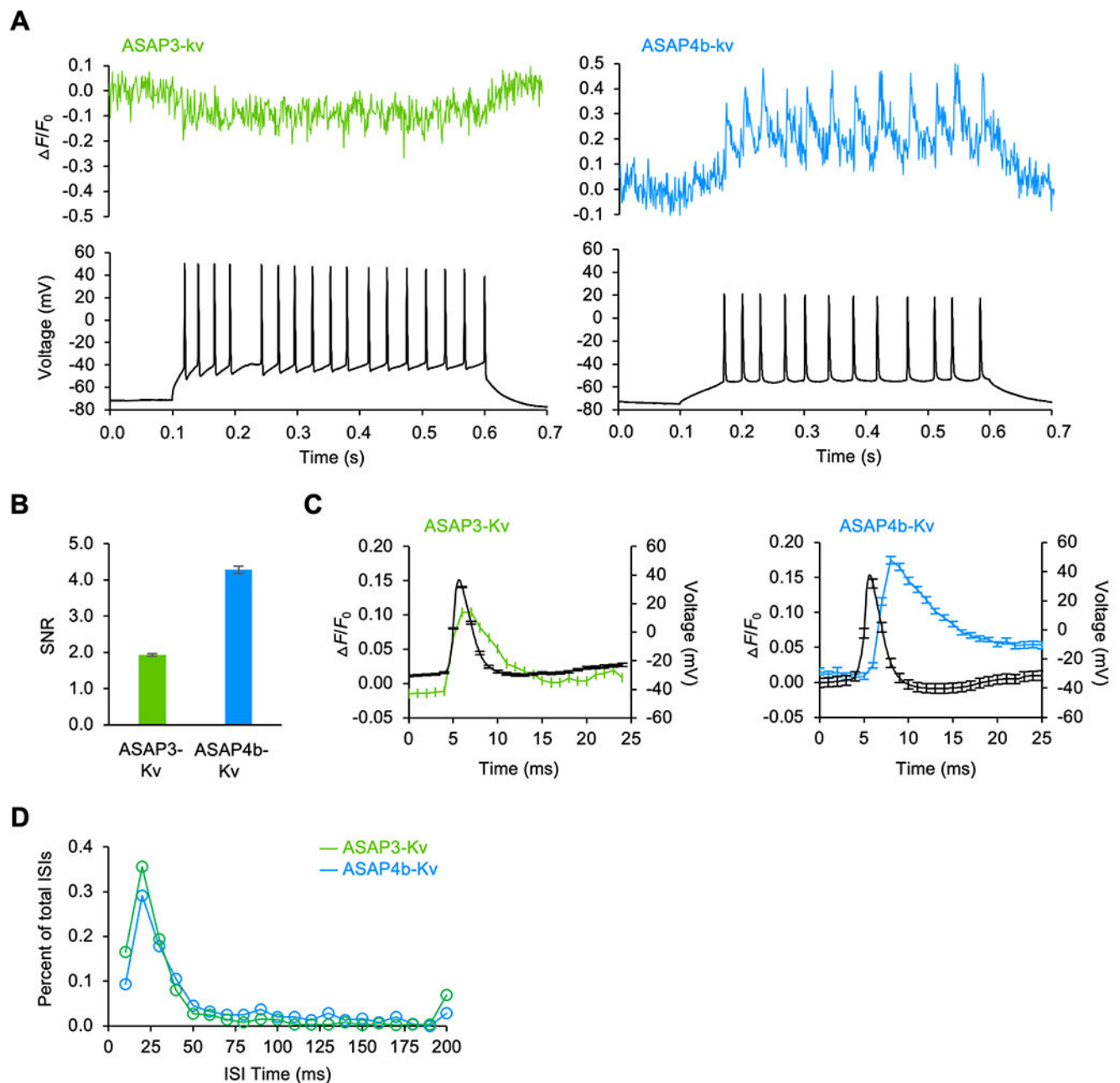
Extended Data Figure 9. ASAP4b-Kv responses to spikes evoked by current steps in hippocampal CA1 pyramidal neurons under two-photon imaging.
(A) Above: raw, uncorrected fluorescence traces, showing example single-trial fluorescence responses to the two indicators in our 2P system for ASAP4b-kv (blue) and ASAP3-kv (green). Below, the corresponding electrophysiological traces for the raw fluorescence traces shown above. (B) Empirical SNR calculated as the ratio of $\Delta F/F_0$ to the SD of F_0 for current step-evoked spikes. Error bars are SEM. ASAP4b-Kv had significantly higher SNR than ASAP3-Kv ($p < 0.0001$ by Mann-Whitney U test). Error bars are SEM. n = 611 spikes for ASAP3-Kv and 284 for ASAP4b-Kv. (C) Average ASAP3-Kv and ASAP4e-Kv

fluorescence responses to current step-evoked spikes of at least 20mV, overlaid over the average voltage response. Time from crossing 20 mV crossing to fluorescence peak was 1.3 ± 1.4 ms (SD) for ASAP3-Kv and 3.6 + 1.3ms for ASAP4b-Kv. Sampling rate was 1 kHz for fluorescence and 10 kHz for electrophysiology. Error bars are SEM. n = 611 spikes for ASAP3-Kv and 284 for ASAP4e-Kv. (**D**) Histogram of the interspike-intervals (ISIs) for each indicator with 10-ms bins. Circles represent actual histogram values.
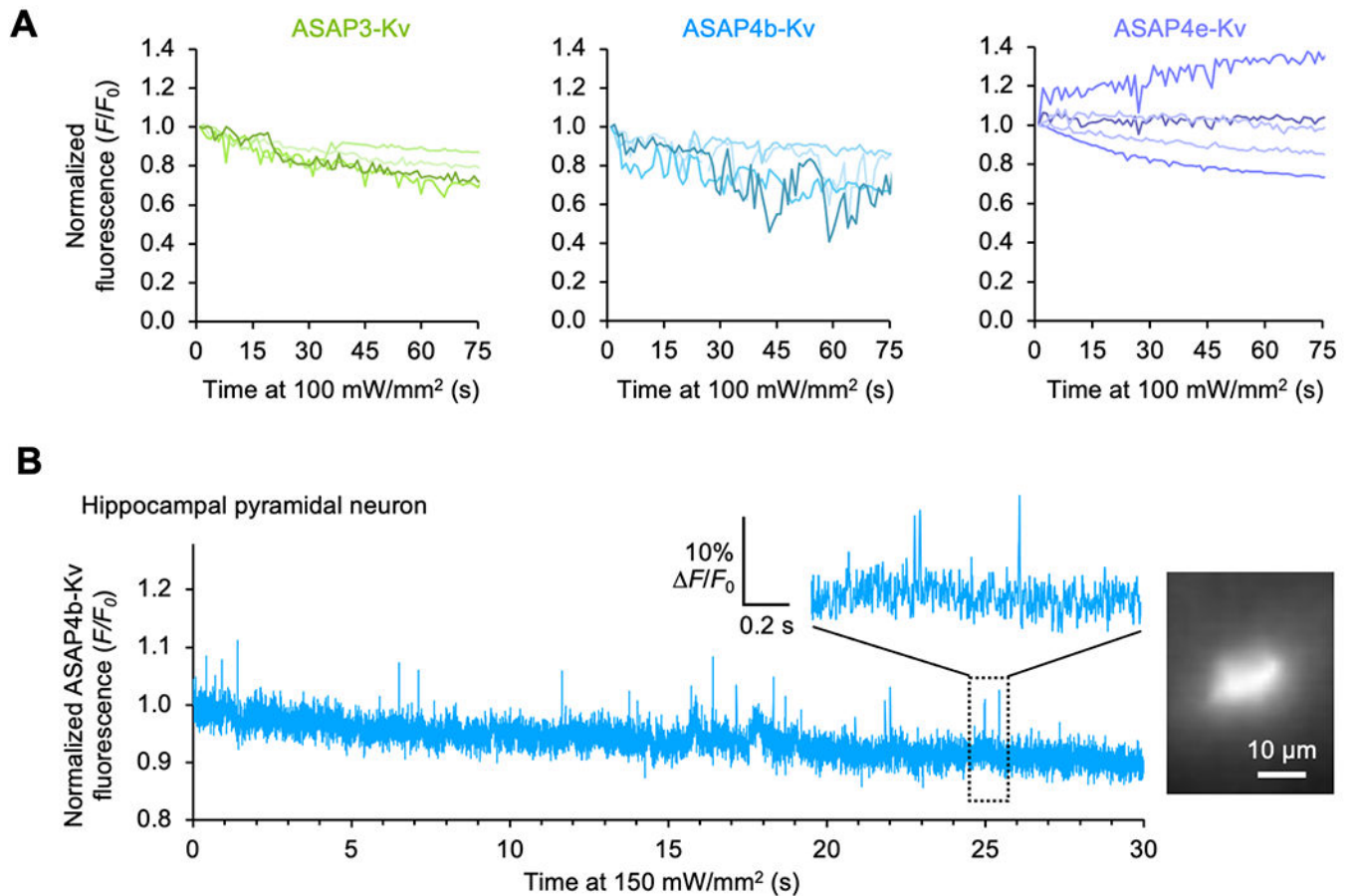
Extended Data Figure 10. In vivo voltage imaging under one-photon wide-field illumination in hippocampus and primary motor cortex.

(**A**) Photostability during continuous one-photon illumination of ASAP3-Kv, ASAP4b-Kv, and ASAP4e-Kv in hippocampal SST+ interneurons *in vivo*. Powers used were 100–250 mW/mm^2, and time coordinates were adjusted to simulate 100 mW/mm^2 assuming linearity between power and photobleaching rate. (**B**) A hippocampal CaMK2α+ neuron expressing ASAP4b-Kv imaged under one-photon illumination (150 mW/mm^2) and its fluorescence trace for 30 seconds. The signals were acquired at 1000-fps and time-binned to 500fps. The trace was normalized to the mean signal of the first 100 frames and not corrected for photobleaching. The rightmost zoomed-in trace shows spontaneous spikes.

Supplementary Material

Refer to Web version on PubMed Central for supplementary material.

Acknowledgements

Data availability

Raw data is available for all figures from the authors upon request. Plasmids for ASAP4b and ASAP4e, along with their sequences, will be deposited at Addgene.

References

1. Antic SD, Empson RM & Knöpfel T Voltage imaging to understand connections and functions of neuronal circuits. J. Neurophysiol 116, 135–152 (2016). [PubMed: 27075539]

2. Zhu MH, Jang J, Milosevic MM & Antic SD Population imaging discrepancies between a genetically-encoded calcium indicator (GECI) versus a genetically-encoded voltage indicator (GEVI). Sci Rep 11, 5295 (2021). [PubMed: 33674659]

3. Helassa N, Podor B, Fine A & Török K Design and mechanistic insight into ultrafast calcium indicators for monitoring intracellular calcium dynamics. Sci Rep 6, 38276 (2016). [PubMed: 27922063]

4. Yang HH & St-Pierre F Genetically Encoded Voltage Indicators: Opportunities and Challenges. J. Neurosci 36, 9977–9989 (2016). [PubMed: 27683896]

5. Brinks D, Klein AJ & Cohen AE Two-Photon Lifetime Imaging of Voltage Indicating Proteins as a Probe of Absolute Membrane Voltage. Biophys. J 109, 914–921 (2015). [PubMed: 26331249]

6. Villette V et al. Ultrafast Two-Photon Imaging of a High-Gain Voltage Indicator in Awake Behaving Mice. Cell 179, 1590–1608.e23 (2019). [PubMed: 31835034]

7. Piatkevich KD et al. A robotic multidimensional directed evolution approach applied to fluorescent voltage reporters. Nat Chem Biol 14, 352–360 (2018). [PubMed: 29483642]

8. Abdelfattah AS et al. Bright and photostable chemigenetic indicators for extended in vivo voltage imaging. Science 365, 699–704 (2019). [PubMed: 31371562]

9. Abdelfattah AS et al. A general approach to engineer positive-going eFRET voltage indicators. Nat Commun 11, 3444 (2020). [PubMed: 32651384]

10. Gong Y et al. High-speed recording of neural spikes in awake mice and flies with a fluorescent voltage sensor. Science 350, 1361–1366 (2015). [PubMed: 26586188]

11. Lou S et al. Genetically Targeted All-Optical Electrophysiology with a Transgenic Cre-Dependent Optopatch Mouse. J. Neurosci 36, 11059–11073 (2016). [PubMed: 27798186]

12. Chamberland S et al. Fast two-photon imaging of subcellular voltage dynamics in neuronal tissue with genetically encoded indicators. Elife 6, e25690 (2017). [PubMed: 28749338]

13. Maclaurin D, Venkatachalam V, Lee H & Cohen AE Mechanism of voltage-sensitive fluorescence in a microbial rhodopsin. Proc. Natl. Acad. Sci. U. S. A 110, 5939–5944 (2013). [PubMed: 23530193]

14. St-Pierre F et al. High-fidelity optical reporting of neuronal electrical activity with an ultrafast fluorescent voltage sensor. Nat Neurosci 17, 884–889 (2014). [PubMed: 24755780]

15. Milosevic MM, Jang J, McKimm EJ, Zhu MH & Antic SD In Vitro Testing of Voltage Indicators: Archon1, ArcLightD, ASAP1, ASAP2s, ASAP3b, Bongwoori-Pos6, BeRST1, FlicR1, and Chi-VSFP-Butterfly. eNeuro 7, ENEURO.0060-20.2020 (2020).

16. Wu J et al. Kilohertz two-photon fluorescence microscopy imaging of neural activity in vivo. Nat Methods 17, 287–290 (2020). [PubMed: 32123392]

17. Webb B & Sali A Comparative Protein Structure Modeling Using MODELLER. Curr Protoc Bioinformatics 54, 5.6.1–5.6.37 (2016).

18. Tsien RY The green fluorescent protein. Annu. Rev. Biochem 67, 509–544 (1998). [PubMed: 9759496]

19. Wang Y, Shyy JY & Chien S Fluorescence proteins, live-cell imaging, and mechanobiology: seeing is believing. Annu Rev Biomed Eng 10, 1–38 (2008). [PubMed: 18647110]

20. Lam AJ et al. Improving FRET dynamic range with bright green and red fluorescent proteins. Nat Methods 9, 1005–1012 (2012). [PubMed: 22961245]

21. Grimm SS & Isacoff EY Allosteric substrate switching in a voltage-sensing lipid phosphatase. Nat Chem Biol 12, 261–267 (2016). [PubMed: 26878552]

22. Barnett L, Platisa J, Popovic M, Pieribone VA & Hughes T A fluorescent, genetically-encoded voltage probe capable of resolving action potentials. PLoS One 7, e43454 (2012). [PubMed: 22970127]

23. Platisa J, Vasan G & Yan A Directed evolution of key residues in fluorescent protein inverses the polarity of voltage sensitivity in the genetically encoded indicator ArcLight. ACS chemical … (2017).

24. Han Z et al. Mechanistic studies of the genetically encoded fluorescent protein voltage probe ArcLight. PLoS One 9, e113873 (2014). [PubMed: 25419571]

25. Akerboom J et al. Crystal structures of the GCaMP calcium sensor reveal the mechanism of fluorescence signal change and aid rational design. J. Biol. Chem 284, 6455–6464 (2009). [PubMed: 19098007]

26. Ning L et al. A Bright, Nontoxic, and Non-aggregating red Fluorescent Protein for Long-Term Labeling of Fine Structures in Neurons. Front Cell Dev Biol 10, 893468 (2022). [PubMed: 35846353]

27. Lim ST, Antonucci DE, Scannevin RH & Trimmer JS A novel targeting signal for proximal clustering of the Kv2.1 K+ channel in hippocampal neurons. Neuron 25, 385–397 (2000). [PubMed: 10719893]

28. Fan JL et al. High-speed volumetric two-photon fluorescence imaging of neurovascular dynamics. Nat Commun 11, 6020 (2020). [PubMed: 33243995]

29. Daigle TL et al. A Suite of Transgenic Driver and Reporter Mouse Lines with Enhanced Brain-Cell-Type Targeting and Functionality. Cell 174, 465–480.e22 (2018). [PubMed: 30007418]

30. Wilt BA, Fitzgerald JE & Schnitzer MJ Photon shot noise limits on optical detection of neuronal spikes and estimation of spike timing. Biophys. J 104, 51–62 (2013). [PubMed: 23332058]

31. Huh CY et al. Excitatory Inputs Determine Phase-Locking Strength and Spike-Timing of CA1 Stratum Oriens/Alveus Parvalbumin and Somatostatin Interneurons during Intrinsically Generated Hippocampal Theta Rhythm. J. Neurosci 36, 6605–6622 (2016). [PubMed: 27335395]

32. Dana H et al. High-performance calcium sensors for imaging activity in neuronal populations and microcompartments. Nat Methods 16, 649–657 (2019). [PubMed: 31209382]

33. Huang L et al. Relationship between simultaneously recorded spiking activity and fluorescence signal in GCaMP6 transgenic mice. Elife 10, (2021).

34. Chen TW et al. Ultrasensitive fluorescent proteins for imaging neuronal activity. Nature 499, 295–300 (2013). [PubMed: 23868258]

35. Dana H et al. Sensitive red protein calcium indicators for imaging neural activity. Elife 5, (2016).

36. Skaggs W, Mcnaughton B & Gothard K An information-theoretic approach to deciphering the hippocampal code. Advances in Neural Information Processing Systems 5, 1030–1030 (1992).

37. Zhang Y et al. Fast and sensitive GCaMP calcium indicators for imaging neural populations. Biorxiv (2021).

38. Koester HJ & Sakmann B Calcium dynamics associated with action potentials in single nerve terminals of pyramidal cells in layer 2/3 of the young rat neocortex. The Journal of physiology 529, 625–646 (2000). [PubMed: 11118494]

39. White MD, Milne RV & Nolan MF A Molecular Toolbox for Rapid Generation of Viral Vectors to Up- or Down-Regulate Neuronal Gene Expression in vivo. Front Mol Neurosci 4, 8 (2011). [PubMed: 21772812]

40. Zolotukhin S et al. Recombinant adeno-associated virus purification using novel methods improves infectious titer and yield. Gene Ther 6, 973–985 (1999). [PubMed: 10455399]

41. Zhang DY, Lau CP & Li GR Human Kir2.1 channel carries a transient outward potassium current with inward rectification. Pflugers Arch 457, 1275–1285 (2009). [PubMed: 19002489]

42. Fan LZ et al. All-optical synaptic electrophysiology probes mechanism of ketamine-induced disinhibition. Nat Methods 15, 823–831 (2018). [PubMed: 30275587]

43. Pfeiffer BD et al. Refinement of tools for targeted gene expression in Drosophila. Genetics 186, 735–755 (2010). [PubMed: 20697123]

44. Rister J et al. Dissection of the peripheral motion channel in the visual system of Drosophila melanogaster. Neuron 56, 155–170 (2007). [PubMed: 17920022]

45. Edelstein A, Amodaj N, Hoover K, Vale R & Stuurman N Computer control of microscopes using μManager. Curr Protoc Mol Biol Chapter 14, Unit14.20 (2010).

46. Schindelin J et al. Fiji: an open-source platform for biological-image analysis. Nat Methods 9, 676–682 (2012). [PubMed: 22743772]

47. Jia H, Rochefort NL, Chen X & Konnerth A Dendritic organization of sensory input to cortical neurons in vivo. Nature 464, 1307–1312 (2010). [PubMed: 20428163]

48. Yang HH et al. Subcellular Imaging of Voltage and Calcium Signals Reveals Neural Processing In Vivo. Cell 166, 245–257 (2016). [PubMed: 27264607]

49. Makinson CD et al. Regulation of Thalamic and Cortical Network Synchrony by Scn8a. Neuron 93, 1165–1179.e6 (2017). [PubMed: 28238546]

50. Ding J, Peterson JD & Surmeier DJ Corticostriatal and thalamostriatal synapses have distinctive properties. J. Neurosci 28, 6483–6492 (2008). [PubMed: 18562619]

51. Carter AG & Sabatini BL State-dependent calcium signaling in dendritic spines of striatal medium spiny neurons. Neuron 44, 483–493 (2004). [PubMed: 15504328]

52. Sun W, Tan Z, Mensh BD & Ji N Thalamus provides layer 4 of primary visual cortex with orientation- and direction-tuned inputs. Nat Neurosci 19, 308–315 (2016). [PubMed: 26691829]

53. Xu F, Shi DQ, Lau PM, Lin MZ & Bi GQ Excitation wavelength optimization improves photostability of ASAP-family GEVIs. Mol Brain 11, 32 (2018). [PubMed: 29866136]

54. Podgorski K & Ranganathan G Brain heating induced by near-infrared lasers during multiphoton microscopy. J. Neurophysiol 116, 1012–1023 (2016). [PubMed: 27281749]

55. Taxidis J et al. Differential Emergence and Stability of Sensory and Temporal Representations in Context-Specific Hippocampal Sequences. Neuron 108, 984–998.e9 (2020). [PubMed: 32949502]

56. Hwang FJ et al. Motor learning selectively strengthens cortical and striatal synapses of motor engram neurons. Neuron 110, 2790–2801.e5 (2022). [PubMed: 35809573]

57. Chien MP et al. Photoactivated voltage imaging in tissue with an archaerhodopsin-derived reporter. Sci Adv 7, eabe3216 (2021). [PubMed: 33952514]

58. Plitt MH & Giocomo LM Experience-dependent contextual codes in the hippocampus. Nat Neurosci 24, 705–714 (2021). [PubMed: 33753945]
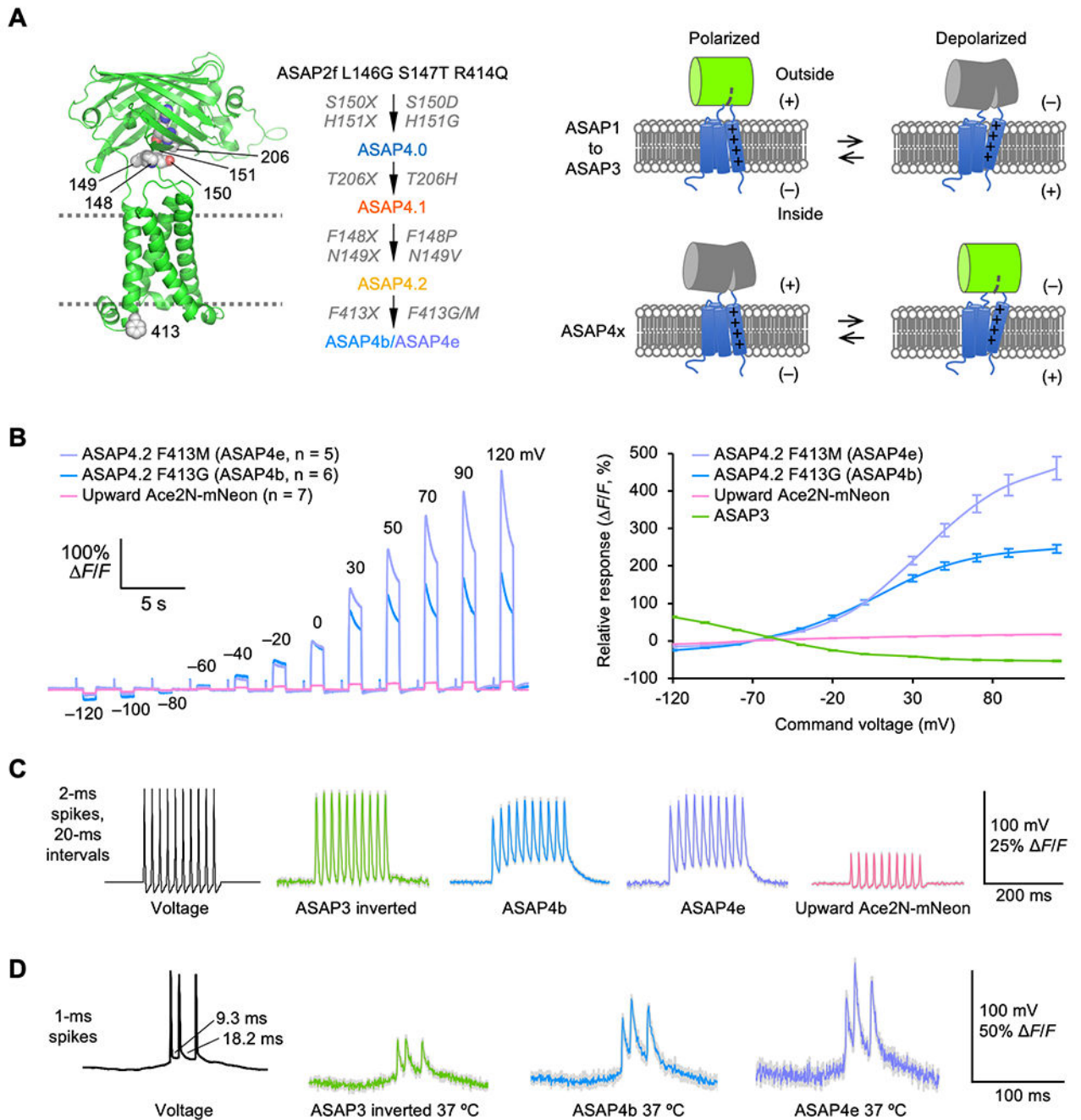
Figure 1. The ASAP4-family of positively tuned GEVIs.

(**A**) Left**,** ASAP4.2 model showing mutated positions. Right, schematics showing reversal of voltage tuning from negative to positive with ASAP4. (**B**) Left, steady-state responses to voltage commands in HEK293A cells of ASAP4.2 F413G (ASAP4b), ASAP4.2 F413M (ASAP4e), and upward Ace2N-mNeon, normalized to −70 mV. Right, resulting *F-V* curves. Error bars, SEM of n = 5 cells for ASAP4b, 6 for ASAP4e, and 7 for upward Ace2mNeon. (**C**) Response to commanded spike trains in HEK293A cells at room temp. V_m was −70 mV at the start of the displayed segment and peak AP amplitude was 100 mV. Responses

were collected from 6 (ASAP4.2), 7 (ASAP4b), 5 (ASAP4e), 6 (ASAP3) and 7 (Upward Ace2mNeon) cells, each supplying a single unfiltered and unsmoothed 1000-Hz trace. Colored lines represent means, gray shading is SEM. **(D)** Responses in HEK293A cells to an AP burst waveform with spike widths of 1.0 ms at FWHM, previously recorded from the mouse hippocampus at 37 °C. V_m was −52 mV at the start of the displayed segment. Each colored line is the mean of 5 HEK293 cells, each supplying a single unfiltered and unsmoothed trace. Gray shading, SEM.
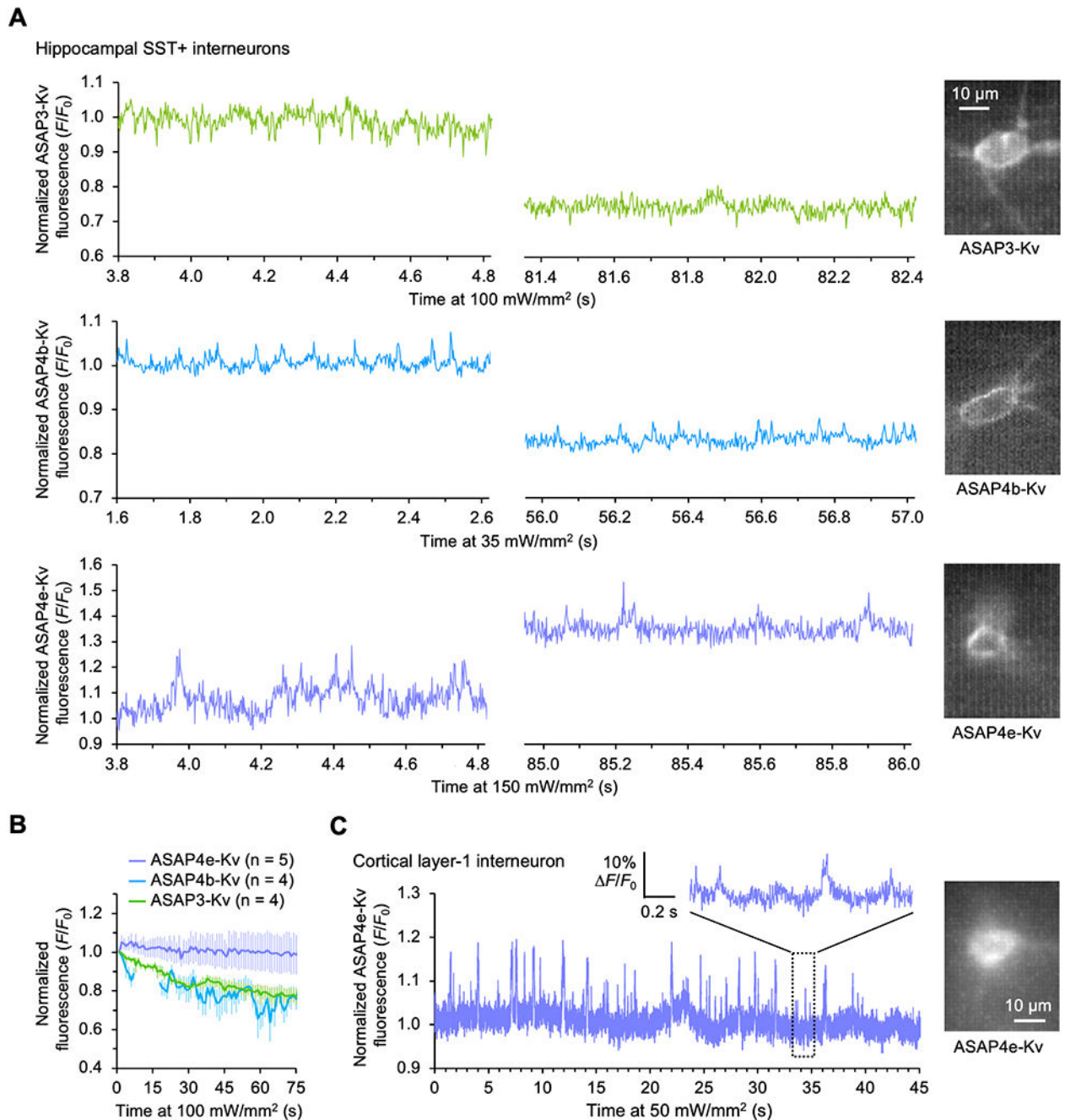
Figure 2. In vivo photostability under one-photon illumination in hippocampal SST+ interneurons.

(**A**) Examples of 1-photon images of ASAP3-Kv, ASAP4b-Kv, and ASAP4e-Kv in hippocampal SST+ interneurons *in vivo*. ASAP3-Kv and ASAP4e-Kv were acquired at 1000 fps in 11-s bouts with 8-s rest periods, then traces were concatenated and time-binned to 500 fps. ASAP4b-Kv was acquired continuously at 400 fps for 60 s. All traces are shown without flattening or filtering. (**B**) Photostability during continuous one-photon illumination of ASAP3-Kv, ASAP4b-Kv, and ASAP4e-Kv in hippocampal SST+ interneurons *in vivo*.

Powers used were 100–250 mW/mm^2, and time coordinates were adjusted to simulate 100 mW/mm^2 assuming linearity between power and photobleaching rate. The ASAP4b-Kv line contains a gap due to severe movement. Error bars represent SEM. (**C**) ASAP4e-Kv signals from a neuron in layer 1 of primary motor cortex imaged for 60 seconds at 384 fps with irradiance of 50 mW/mm^2. The first 15 s of the recording was removed for analysis to exclude motion artifacts. The trace was normalized to the mean signal of the first 0.26 s and not flattened or filtered.
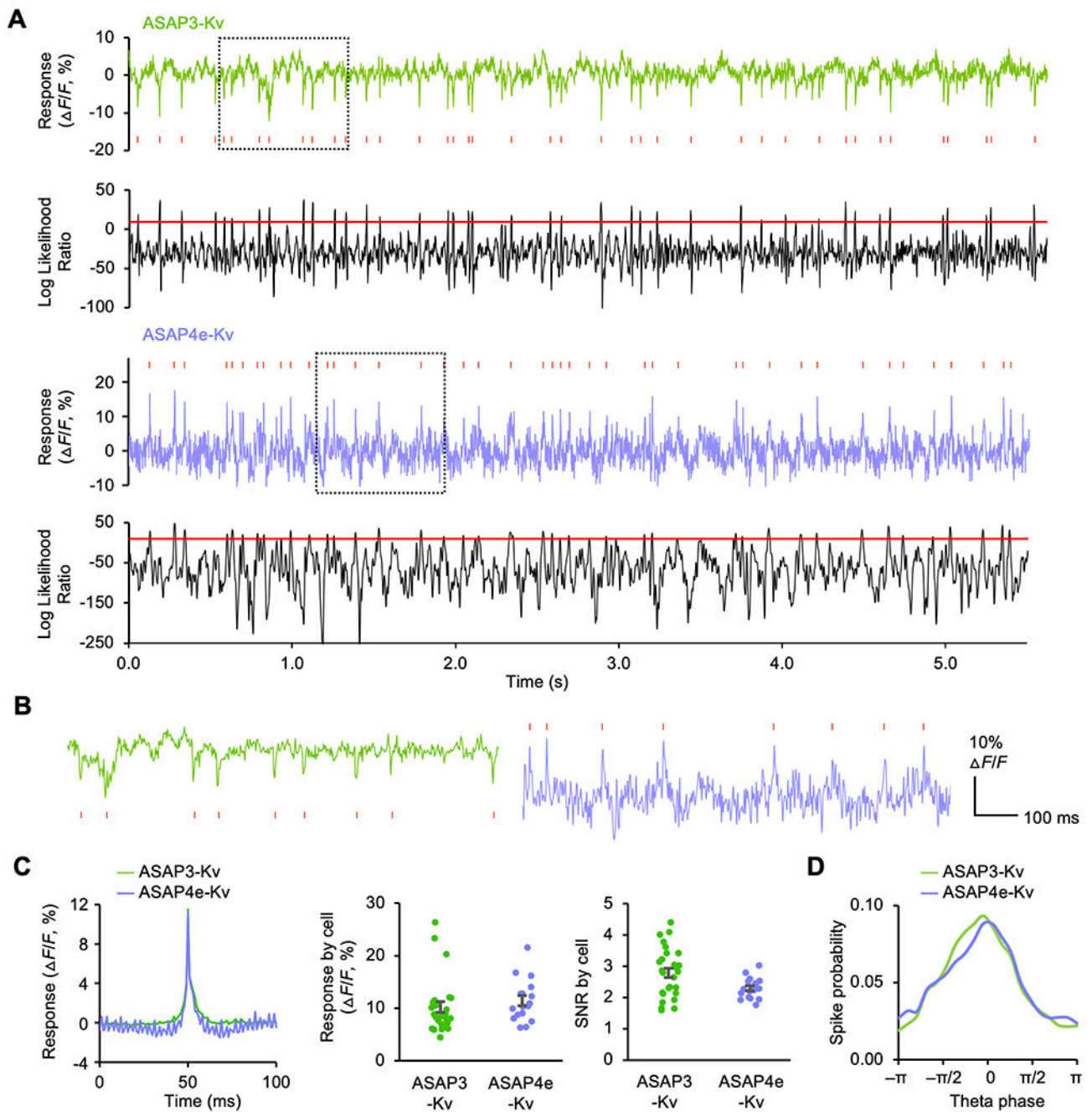
Figure 3. One-photon imaging of ASAP GEVIs in hippocampal SST+ interneurons in vivo.
(**A**) Example GEVI traces recorded at 1000 fps and 100 mW/mm^2, then time-binned to 500 fps and flattened, but not filtered, and corresponding log likelihood ratio probability traces with the AP detection threshold drawn as a red line. (**B**) Expanded view of the boxed regions in (A). (**C**) Spike metrics from 28 ASAP3-Kv cells and 17 ASAP4e-Kv cells. To compare indicators without confounding by photobleaching, only data from the first 11 s of each recording was used. Left, the average waveform of detected spikes, with the response direction of ASAP3-Kv flipped for comparison. Middle, the average response size $\Delta F/F_0$

by cell. Bars represent mean ± SEM. ASAP3-Kv values are reversed. The difference was not significant (p = 0.0992 Mann-Whitney test). Right, empirically calculated SNR per cell. Bars represent mean ± SEM. SNR was calculated on unfiltered data, then corrected to simulate 100 mW/mm^2 under Poisson assumptions to account for differences in illumination intensity between cells. **(D)** Histogram of spike probability over theta phase. Phase was broken into 20 timing bins from 0 to 2π radians in the theta band, defined as 6 to 11 Hz. ASAP3-Kv contributed 10886 spikes from 28 cells, while ASAP4e-Kv contributed 6588 spikes from 17 cells. Both indicators revealed a similar trend for spike preference near the peak at 0 radians.
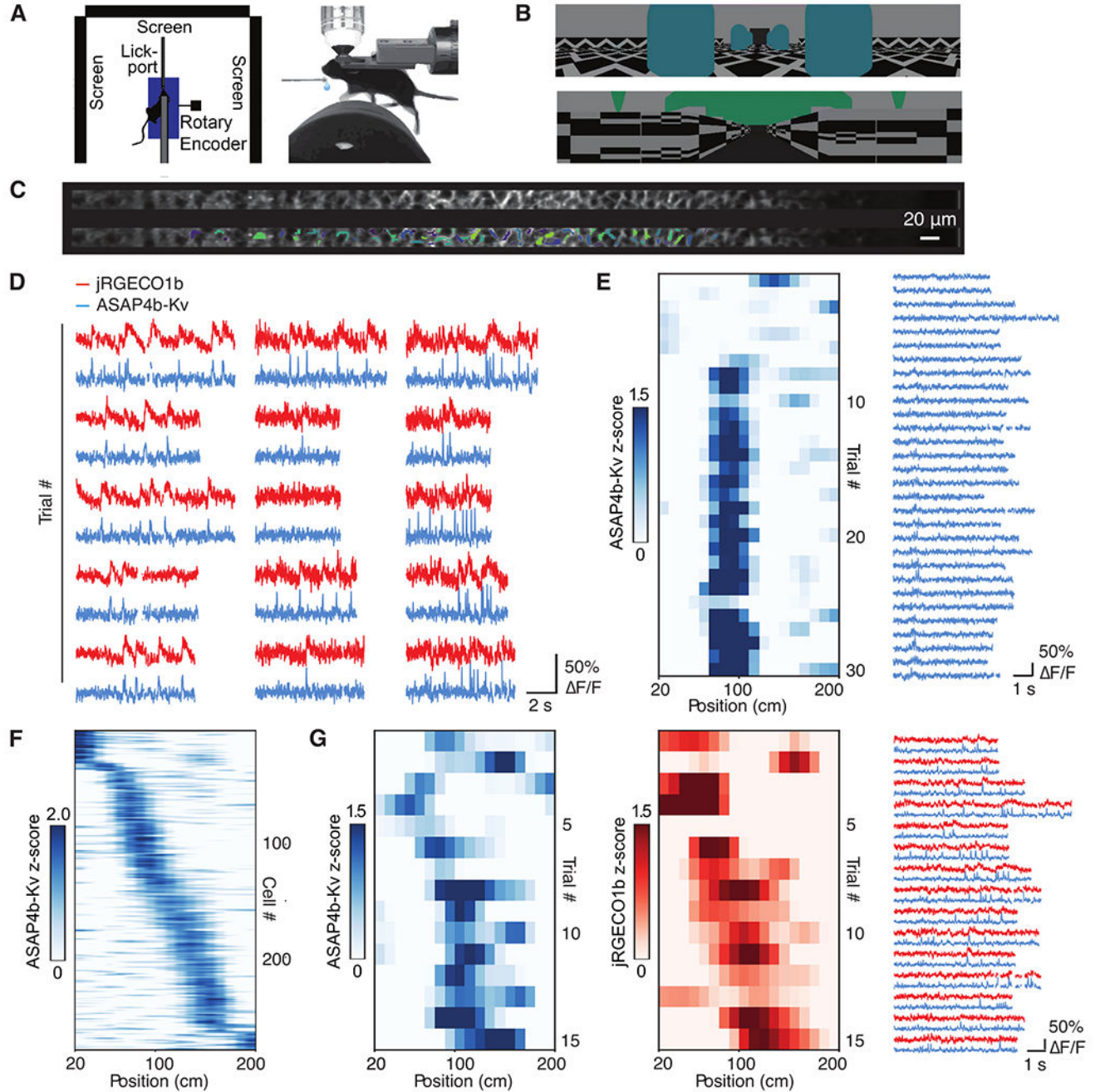
Figure 4. Precision mapping of hippocampal place cells by voltage imaging.
(**A**) A head-fixed mouse runs on a cylinder whose rotation is translated to movement through a virtual environment displayed on three screens surrounding the mouse. (**B**) The mouse's view at the beginning of the two virtual tracks used for data collection. Data was pooled across both environments. (**C**) Example ASAP image without (top) and with (bottom) ROIs highlighted. (**D**) Simultaneously recorded 989-fps ASAP4b-Kv and jRGECO1b F/F_0 traces from a subset of trials in a single session, showing highly correlated ASAP4b-Kv and jRGECO1b transients with different kinetics. Each column is a different ROI. Some

frames are missing due to brain motion. **(E)** Example place-selective ROI from the FOV shown in (C). Left, heatmap indicates ASAP4b-Kv fluorescene within each spatial bin on each trial. Position-binned fluorescence values were z-scored across all trials. Right, F/F_0 traces corresponding to these trials. Traces are of different durations due to different running speeds. Trials occurred in a single session and included a total of 240 s of imaging. **(F)** Trial-averaged (bootstrapped) ASAP4b-Kv activity of every place-selective ROI as a function of position (n = 283 ROIs) across all mice (n = 3) and imaging sessions. Each row indicates the activity of a single ROI. ROIs are sorted by their location of peak activity. **(G)** Left, trial x position activity rate maps from a place cell exhibiting patterns of activity in both ASAP4b-Kv and jRGECO1b channels with place preferences. Right, F/F_0 traces corresponding to these trials. Traces are of different durations due to different running speeds.
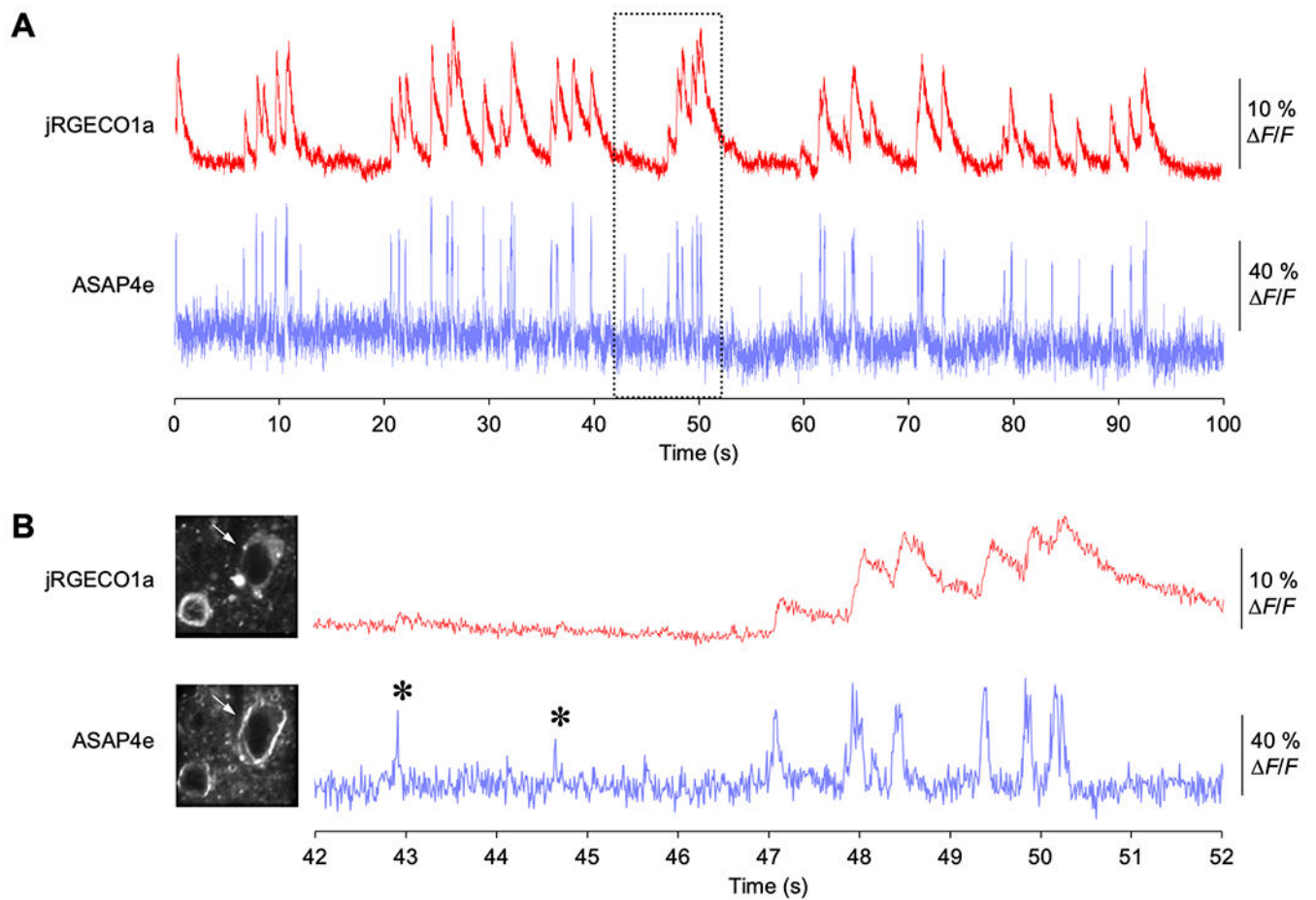
Figure 5. Simultaneous voltage and calcium imaging in cortical pyramidal neurons in vivo.
(A) ASAP4e-Kv and jRGECO1a were co-expressed in layer-2 cortical neurons of mice. Imaging was done through a cranial window over V1 with a standard resonant galvanometer-based scanner at 99 fps using a wavelength of 1000 nm to excite both ASAP4e-Kv and jRGECO1a simultaneously, despite 1000nm being suboptimal for ASAP4e. Traces shown have been normalized to 1 by dividing by the average of seconds 4-5, but are otherwise unmodified and uncorrected for photobleaching so that photobleaching may be observed, and represent raw and unfiltered data. The dashed box represents the zoomed in portion in panel B. **(B)** Inset of the dashed box from (A). Asterisks mark voltage events that show little to no response in the calcium (jRGECO1a) channel. Between 47 s and 51 s, ASAP4e-Kv tracks bursts of electrical events with better temporal resolution than jRGECO1a, with ASAP4e-Kv peaks preceding the jRGECO1a peaks.

Table 1.

Relative fluorescence per molecule of ASAP4 variants

	V_{half} (mV)[*]	Per-molecule fluorescence at −70 mV ($mF_0 = F_{−70}/F_{max}$)	Per-molecule fluorescence at +30 mV (F_{+30}/F_{max})	Per-molecule fluorescence change, 100 mV ($m\Delta F = \Delta F_{100}/F_{max}$)	Per-molecule SNR determinant ($m\Delta F/mF_0^{1/2}$)	Relative fluorescence change, 100 mV ($\Delta F_{100}/F_0$, %)	Relative fluorescence change, 1 AP ($\Delta F_{AP}/F_0$, %)[**]
ASAP3	−90	0.52	0.27	0.25	0.35	48	25
ASAP4.0	49	0.17	0.46	0.29	0.70	170	37
ASAP4.1	−34	0.56	0.91	0.35	0.47	63	26
ASAP4.2	−17	0.42	0.83	0.41	0.64	98	28
ASAP4.2 F413A	−10	0.40	0.84	0.44	0.70	110	ND
ASAP4b	2.8	0.27	0.75	0.48	0.93	180	35
ASAP4e	36	0.17	0.53	0.36	0.87	210	38

[*] Midpoint of fluorescence-voltage curve fit to a Boltzmann function.

[**] $\Delta F/F_0$ fluorescence change per action potential waveform (FWHM = 3.5ms, amplitude = 100mV) by voltage patch clamp in HEK293 cells.